https://doi.org/10.5194/acp-2022-506
Preprint. Discussion started: 4 August 2022
© Author(s) 2022. CC BY 4.0 License.

Atmospheric Chemistry and Physics Discussions

Using OCO-2 column CO_2 retrievals to rapidly detect and estimate biospheric surface carbon flux anomalies

Andrew F. Feldman[1,2], Zhen Zhang[3], Yasuko Yoshida[4], Abhishek Chatterjee[5], Benjamin Poulter[1]

[1]Biospheric Sciences Laboratory, NASA Goddard Space Flight Center, Greenbelt, MD, 20771, USA
[2]NASA Postdoctoral Program, NASA Goddard Space Flight Center, Greenbelt, MD, 20771, USA
[3]Earth System Science Interdisciplinary Center, University of Maryland, College Park, MD, 20740, USA
[4]Science Systems and Applications, Inc. (SSAI), Lanham, MD, 20706, USA
[5]Jet Propulsion Laboratory, California Institute of Technology, Pasadena, CA, 91109, USA

Correspondence to: Andrew F. Feldman (afeld24@mit.edu)

Abstract. The global carbon cycle is experiencing continued perturbations via increases in atmospheric carbon concentrations. Greenhouse gas satellites that are designed to retrieve atmospheric carbon concentrations can help observe seasonal to interannual variations and sources of carbon dioxide. Recent work has shown that these satellites are further applicable beyond their design specifications for directly identifying and quantifying surface emissions at various spatiotemporal scales. For example, simple mass balance approaches have been used to rapidly estimate surface methane fluxes from satellite atmospheric column methane retrievals. However, less attention has been placed on using satellite column CO_2 retrievals to evaluate surface CO_2 fluxes from the terrestrial biosphere at shorter timescales without inversion models. Such applications could be useful to monitor, in near-real time, biosphere carbon fluxes during climatic anomalies like drought, heatwaves, and floods, before more complex terrestrial biosphere model outputs become available. Here, we explore the ability of Orbiting Carbon Observatory-2 (OCO-2) column-averaged dry air CO_2 (XCO_2) retrievals to directly detect and estimate terrestrial biosphere CO_2 flux anomalies using a simple mass balance approach. Using CarbonTracker model reanalysis as a testbed, we first demonstrate that a previously developed, mass balance approach can estimate monthly surface CO_2 flux anomalies from XCO_2 enhancements in the Western United States. The method is optimal when the chosen target region is spatially extensive enough to account for atmospheric mixing and has favorable advection conditions with contributions primarily from one background region. While errors in individual soundings partially reduce the ability of OCO-2 XCO_2 to estimate more frequent, smaller surface CO_2 flux anomalies, we find that OCO-2 XCO_2 can often detect and estimate larger surface flux anomalies. OCO-2 is thus useful for near real time monitoring of the monthly timing and magnitude of regional terrestrial biosphere carbon anomalies. Any noise reduction in forthcoming greenhouse gas satellites and/or the existence of large surface carbon anomalies will likely enhance the ability to rapidly estimate surface fluxes at smaller spatiotemporal scales.

https://doi.org/10.5194/acp-2022-506
Preprint. Discussion started: 4 August 2022
© Author(s) 2022. CC BY 4.0 License.

Atmospheric Chemistry and Physics Discussions

1 Introduction

With ongoing anthropogenic emissions, atmospheric carbon concentrations continue to rise and alter the global climate system (Friedlingstein et al., 2022). Given many diverse carbon sources and sinks as well as transport of atmospheric carbon, it is a challenge to monitor these atmospheric carbon concentrations and carbon fluxes across the globe. Carbon measurement networks are available, but are spatially biased toward mid-latitude locations with little coverage in the tropics (Schimel et al., 2015a). Therefore, atmospheric transport model assimilation efforts and land surface models are often used to quantify and monitor global carbon sources and sinks (Ott et al., 2015; Peters et al., 2007). However, these datasets typically have a longer latency and complex sources of error due to modeling assumptions about uncertain surface carbon flux drivers.

Greenhouse gas satellites provide an ability to retrieve atmospheric column carbon concentrations and constrain global carbon cycle processes. Over the past two decades, satellite instruments such as SCanning Imaging Absorption spectroMeter for Atmospheric CartograpHY (SCIAMACHY), Greenhouse Gases Observing Satellite (GOSAT), and Orbiting Carbon Observatory-2 (OCO-2) have provided measurements of dry-air column carbon dioxide (XCO_2) and in many cases also methane (XCH_4) (Bovensmann et al., 1999; Eldering et al., 2017b; Kuze et al., 2014; Reuter et al., 2011). These satellites have indeed provided observational constraints on carbon-cycle seasonal and interannual variability with global coverage as desired beyond irregular spatial coverage of in-situ networks (Chen et al., 2021; Lindqvist et al., 2015). Additionally, since these column retrievals are partly a function of surface carbon fluxes (Keppel-Aleks et al., 2012), previous studies have assimilated these XCO_2 and XCH_4 retrievals into atmospheric inversion model frameworks to improve surface carbon flux estimates (Basu et al., 2013; Chevallier et al., 2014; Fraser et al., 2014; Halder et al., 2021; Houweling et al., 2015; Liu et al., 2017; Ott et al., 2015; Zabel et al., 2014).

It has not been widely investigated whether satellites like OCO-2 can directly monitor the timing and magnitude of shorter monthly timescale climate-carbon feedback events, such as those that evolve in the terrestrial biosphere and generate regional and short-lived XCO_2 enhancements. OCO-2 was designed to observe regional-scale carbon sources and sinks to provide a constraint on carbon cycle seasonal and interannual variability (Crisp et al., 2004; Eldering et al., 2017b). Despite initial concern that the noise level of individual soundings would prevent direct monitoring of surface CO_2 flux evolution at finer scales (Chevallier et al., 2007; Eldering et al., 2017a; Miller et al., 2007), there is growing evidence that satellite XCO_2 retrievals can directly detect and monitor surface carbon sources on smaller spatiotemporal scales. For example, many studies have demonstrated that OCO-2 and other satellites can detect anthropogenic emission plumes from urban areas using spatially adjacent satellite soundings (Hakkarainen et al., 2016; Irakulis-Loitxate et al., 2021; Kort et al., 2014; Nassar et al., 2017; Reuter et al., 2019; Schwandner et al., 2017; Zheng et al., 2020). For natural emission sources, these satellites are typically used to evaluate effects of an event averaged over seasons or multiple years, such as El Niño Southern Oscillation events and related biomass burning (Byrne et al., 2021; Chatterjee et al., 2017; Eldering et al., 2017b; Hakkarainen et al., 2019; Heymann

https://doi.org/10.5194/acp-2022-506
Preprint. Discussion started: 4 August 2022
© Author(s) 2022. CC BY 4.0 License.

Atmospheric Chemistry and Physics Discussions

et al., 2016; Liu et al., 2018; Patra et al., 2017). However, recent studies interpret monthly XCO_2 anomalies (from OCO-2) without inversion models to understand evolution of a flood event (Yin et al., 2020) and ocean and terrestrial biosphere carbon cycle co-evolution during the 2015-2016 El Niño (Chatterjee et al., 2017). As such, satellite XCO_2 shows promise for directly monitoring the monthly timing and evolution of regional carbon-climate feedbacks from the biosphere at smaller spatiotemporal scales without model assimilation frameworks. Directly observing surface fluxes with satellite XCO_2 would allow rapid detection, monitoring, and/or estimation of surface CO_2 fluxes, which are only sparsely observed with ground networks and become available at longer latency from modeling efforts (Schimel et al., 2015a)

A main consideration of evaluating XCO_2 over smaller spatiotemporal scales is whether the surface carbon perturbation to XCO_2 is above the XCO_2 retrieval noise level. Surface carbon sources and sink anomalies ultimately need to be detected within a high background XCO_2 variability, driven by atmospheric transport as well as surface fluxes (Basu et al., 2018; Hakkarainen et al., 2016). The observed XCO_2 anomalies are typically under 2 ppm (Hakkarainen et al., 2019). Furthermore, XCO_2 anomalies attributed to the most extreme surface perturbations may be below 1 ppm (Chatterjee et al., 2017; Crisp et al., 2017; Miller et al., 2007; Weir et al., 2021). However, GOSAT and SCIAMACHY XCO_2 retrievals have estimated uncertainty over 1 ppm (Buchwitz et al., 2017a; Butz et al., 2011), which limits their ability to interpret even the strongest monthly XCO_2 anomalies due to surface fluxes. By contrast, OCO-2 XCO_2 uncertainty is between 0.5 and 1 ppm for a given sounding (Eldering et al., 2017b; Wunch et al., 2017). With its greater number of daily soundings and higher resolution, aggregated regional-scale XCO_2 uncertainty can decrease below 0.5 ppm (Chatterjee et al., 2017). This precision has allowed detection of regional declines in fossil fuel emissions on the order of 0.25-0.5 ppm during the COVID-19 pandemic (Weir et al., 2021), with caveats of limited anomaly detection on the lower end of this range (Buchwitz et al., 2021; Chevallier et al., 2020). As such, OCO-2 may provide an ability to monitor the evolution of smaller regional surface sources and sinks of CO_2 more precisely at monthly timescales than previous spaceborne greenhouse gas instruments.

Recently, XCH_4 retrievals have been used to rapidly estimate surface methane fluxes using simple mass balance approaches (Buchwitz et al., 2017b; Pandey et al., 2021). These methods do not require transport models and perform reasonably well. However, it is unclear whether such an approach can be used for surface fluxes – CO_2 fluxes tend to have more spatially homogenous surface sources and sinks compared to more spatially heterogeneous CH_4 fluxes. Nearly all efforts to estimate surface CO_2 fluxes from OCO-2 XCO_2 retrievals have involved transport models and inversions (Byrne et al., 2021; Liu et al., 2017; Palmer et al., 2019; Patra et al., 2017). The few studies estimating surface emissions directly from the XCO_2 anomalies alone are empirical (rather than physically-based mass balance methods) in using model-based relationships between XCO_2 and surface CO_2 fluxes (Heymann et al., 2016) or are specific to point source plumes at under kilometer scales rather than hundreds of kilometer scale areal sources (Zheng et al., 2020).

https://doi.org/10.5194/acp-2022-506
Preprint. Discussion started: 4 August 2022
© Author(s) 2022. CC BY 4.0 License.

Atmospheric Chemistry and Physics Discussions

An equivalent approach using XCO_2 in a mass balance would provide an ability to rapidly estimate regional total carbon flux anomalies from the terrestrial biosphere, which are difficult to estimate given their many contributions and require sophisticated models. Specifically, such a method could allow near real time monitoring of the duration, magnitude, and spatial extent of CO_2 flux anomalies during extreme climatic events (Frank et al., 2015; Reichstein et al., 2013). Such applications are especially important for regional climate change hotspots like in the southwestern North America where droughts and heatwaves are becoming more frequent and intense (Cook et al., 2015; Schwalm et al., 2012; Williams et al., 2022). Analogously, a simple approach for estimating ecosystem water fluxes (i.e., triangle method; Carlson, 2007) has a legacy of continued use given its relatively sufficient accuracy for many applications compared to more complex land surface model approaches. Given the ongoing challenges of estimating surface fluxes at large spatial scales, we anticipate that it will be similarly useful to develop simple total surface carbon flux estimation approaches that are rapid, rely on observations alone (from remote sensing), do not require many modeling assumptions and ancillary data, and provide an independent estimate to evaluate model outputs.

Here, we ask: can satellite retrieved XCO_2 be used with mass-balance approaches to directly detect and estimate terrestrial surface CO_2 flux anomalies, especially from the biosphere? Can surface CO_2 flux anomalies be monitored with XCO_2 at sub-seasonal (i.e., monthly) scales? Which wind and spatial domain conditions are most suitable for coupling between XCO_2 and surface CO_2 fluxes such that XCO_2 can be used to estimate surface CO_2 fluxes? OCO-2 is chosen due mainly to its high precision and greater sensitivity to the lower atmosphere, which makes it more sensitive to surface fluxes than other greenhouse gas satellites (Eldering et al., 2017a). Recent algorithmic updates have also been shown to increase OCO-2 XCO_2 retrievals' representation of biospheric fluxes at subcontinental scales (Miller and Michalak, 2020).

Addressing these questions here can help assess whether greenhouse-gas satellites can be used to monitor biosphere carbon responses to climatic anomalies at sub-seasonal timescales and in near real time (within 1–2-month latency). For example, greenhouse gas satellite XCO_2 anomalies could be used as an initial assessment of an ongoing extreme event and guide more holistic monitoring and attribution of the event with other observational and model tools. This would provide a rapid carbon cycle monitoring capability not available with global models and sparse networks that have a lack of spatial coverage and/or longer latency (Ciais et al., 2014). These questions will also assess our ability to rapidly estimate regional biosphere fluxes in climate change hotspots as well as in the tropics (Byrne et al., 2017) which sequester the most fossil fuels but lack measurement networks (Liu et al., 2017; Schimel et al., 2015b).

2 Methodology

https://doi.org/10.5194/acp-2022-506
Preprint. Discussion started: 4 August 2022
© Author(s) 2022. CC BY 4.0 License.

Atmospheric Chemistry and Physics Discussions

2.1 Region Selection

We evaluate the Western US (latitude of 33° N to 49° N and longitude of 124° W to 104° W) given its extent of natural ecosystems that serve as a carbon sink as well as the fact that it has become a hotspot for droughts, including an ongoing decadal-scale megadrought (Cook et al., 2015; Schwalm et al., 2012; Williams et al., 2022). In this region, we expect that terrestrial biosphere fluxes (i.e., photosynthesis, respiration, wildfire) will dominate CO_2 surface flux anomalies rather than anthropogenic fluxes. We later show that this region additionally has favorable advection conditions for using XCO_2 to assess surface fluxes (see Sect. 3.1).

2.2 Datasets

The study includes three components to assess the potential for using XCO_2 to directly evaluate monthly surface flux anomalies. We first evaluated advection conditions where we use the modern-era retrospective analysis for research and applications, version 2 (MERRA2) wind vectors between the surface and 700 mb, which approximately captures the boundary layer (Gelaro et al., 2017; GMAO, 2015). In this study, we refer to advection as the horizontal transport of air, especially that in the boundary layer. This lower troposphere layer directly interacts with the surface fluxes that influence XCO_2 (Buchwitz et al., 2017b; Pandey et al., 2021).

Second, we tested the ability of XCO_2 to estimate surface CO_2 fluxes using CarbonTracker model reanalysis (CT2019B) as a testbed, which assimilates tower eddy flux and satellite atmospheric radiance observations into an atmospheric transport model and outputs hourly XCO_2 and total surface CO_2 fluxes from 2000 to 2018 (Peters et al., 2007). Tests performed using this model reanalysis dataset are meant to represent simulated "true" relationships between surface fluxes and XCO_2 dynamics. However, we acknowledge model errors in this framework. A purely simulated environment with error free conditions is not possible here because coupling between surface CO_2 fluxes and XCO_2 require modeling and assumptions about atmospheric transport and emission physics. Therefore, we recognize that error in estimating surface CO_2 fluxes from XCO_2 will be partially a function of errors in modeling assumptions beyond that of errors in the simple mass balance approach.

Third, we assessed the ability of observed XCO_2 between September 2014 and July 2021 from the Orbiting Carbon Observatory 2 (OCO-2) to detect and estimate surface fluxes using mass balance (Eldering et al., 2017b). OCO-2 has an approximate 3 km^2 resolution per sounding and 16-day revisit cycle with soundings at around 1:30 pm local time. We use OCO-2 level 2, bias-corrected, retrospective reprocessing version 10 of XCO_2 (OCO-2-Science-Team et al., 2020). Quality flags were used to remove soundings with poor retrievals. Observations of total surface CO_2 fluxes are only sparsely located in space. We, therefore, independently estimated surface fluxes from a biosphere model, fire reanalysis, and anthropogenic emission repositories. The Lund-Potsdam-Jena (LPJ) dynamic global vegetation model was driven with MERRA2 reanalysis forcing to output CO_2 flux from net biome production (NBP) between January 1980 and July 2021 (Gelaro et al., 2017; Sitch

https://doi.org/10.5194/acp-2022-506
Preprint. Discussion started: 4 August 2022
© Author(s) 2022. CC BY 4.0 License.

Atmospheric Chemistry and Physics Discussions

et al., 2003; Zhang et al., 2018). NBP models carbon fluxes from photosynthesis, respiration, land use change, and fire. Since LPJ only evaluates fire dynamics at the annual scale and wildfire can rapidly evolve over widespread areas in the Western US, fire carbon fluxes were obtained from Quick Fire Emissions Dataset (QFED) biomass burning emissions between 2000 and 2021 to account for monthly fire dynamics in the total carbon fluxes (Koster et al., 2015). LPJ NBP annual fire emissions were removed from the total NBP and monthly QFED biomass burning emissions were added. Anthropogenic CO_2 fluxes were obtained from CarbonMonitor for the Western US region between 2019 and 2021 (Liu et al., 2020). MODIS-based FluxSat gross primary production (GPP), though only evaluating photosynthesis and no respiration or disturbance components, provides another independent observation-based surface flux estimate to determine coupling between XCO_2 and biospheric fluxes (Joiner and Yoshida, 2021, 2020).

2.3 Wind Vector Analysis

We assessed monthly averaged MERRA2 wind vectors between the surface and 700 mb across the Western US. We specifically used the eastward and northward wind fields from the MERRA2 assimilated meteorological fields (M2T3NVASM) (Gelaro et al., 2017). We first visually evaluated wind quiver plots. Next, the spatially averaged wind direction and speed were determined within the region and at each of its four borders. The average (or, here, "total") wind velocity is determined within the region by averaging the velocity from all pixels in the region. The speed of winds entering the region at each border were computed by determining only the average velocity component of the wind entering the region. For example, at the western border, the eastward wind velocity component of the pixels along the western border of the domain were averaged. Finally, the percentage of the background region's boundary layer air entering the domain for each of its four borders was estimated as the ratio of the wind vector component entering the region to the total wind vector. For example, at the western border of the domain, this percentage is computed as the speed of the eastward component of the wind velocity divided by the total velocity at the border. Negative values are set to zero to indicate that air from that background region does not enter the target domain on average.

2.4 XCO_2-Based Surface Flux Estimation

First, XCO_2 and CO_2 surface fluxes in all cases were averaged to monthly and spatially averaged within the Western US target region. Monthly XCO_2 and CO_2 surface fluxes were deseasonalized by averaging all months in the available time series into an average 12-month climatology (i.e., all January values were averaged, all February values were averaged, and so on). This average climatology was subtracted from the raw time series to create an anomaly time series. Given that XCO_2 includes a strong annual increasing trend, each of the twelve months were individually, linearly detrended first before deseasonalizing as in Chatterjee et al. (2017).

https://doi.org/10.5194/acp-2022-506
Preprint. Discussion started: 4 August 2022
© Author(s) 2022. CC BY 4.0 License.

Atmospheric Chemistry and Physics Discussions

Total surface CO_2 flux anomalies were estimated from XCO_2 anomalies in the Western US using a simple mass balance approach previously applied to methane fluxes (Buchwitz et al., 2017b; Jacob et al., 2016; Varon et al., 2018). It was similarly used here to estimate surface CO_2 fluxes (Q; in units of TgC/mo) using:

$$Q = (\Delta XCO_2)(V)(L)(C)\left(M_{exp}\right)(M) \quad (1)$$

ΔXCO_2 (ppm) is the difference in XCO_2 between the target domain (here, the Western US) and the background region where the majority of the incoming winds originate. V is the ventilation wind velocity (in m/s units, but converted to km/month), which has been motivated previously to be best represented by boundary layer winds (Buchwitz et al., 2017b; Pandey et al., 2021). Thus, while the full column CO_2 concentrations were evaluated, the wind speeds in the lower atmosphere are considered in the mass balance model given their greater degree of interaction with the CO_2 fluxes at the surface. Here, V is represented as the monthly averaged boundary layer wind speed within the target region. For the observation-based analysis, MERRA2 wind fields are used while for the reanalysis framework study, CarbonTracker wind velocity outputs are used. L is the effective region length (km) meant to estimate the horizontal pathlength of the ventilation wind passing through the region and interacting with the surface flux. L can be estimated by the square root of the target region area. The model parameter, C, represents a model mass balance assumption that CO_2 fluxes are spatially homogenous, and the ventilation wind is uniform and consistent across the region. This means there is a consistent, linear increase of XCO_2 spatially (from east to west in the Western US region) as the horizontal winds move over a surface CO_2 efflux. C is equal to 2 (unitless) under this assumption where the difference between XCO_2 at the entrance and exit of the region (from the perspective of the horizontal wind) is twice that of the spatially averaged ΔXCO_2. M_{exp} (unitless) is an adjustment of the surface pressure, or the ratio of the target region's surface pressure to standard atmospheric pressure. For the observation-based analysis, MERRA2 surface pressure is used while in the analysis using the reanalysis testbed, CarbonTracker surface pressure outputs are used. M converts the atmospheric carbon dioxide mixing ratio (or its concentration) to a total column mass considering the volume of the atmospheric column overlying the target region's land surface. It additionally includes a conversion from CO_2 to its carbon equivalent. M is therefore 4.2×10^{-6} TgC/(km^2 $ppmCO_2$).

Previous demonstrations of Eq. 1 on methane fluxes evaluated the raw, rather than anomaly, XCH_4 enhancements (Buchwitz et al., 2017b; Pandey et al., 2021). In the main analysis, we have removed XCO_2 seasonality here due to many sources of seasonal atmospheric CO_2 variability (atmospheric and surface-based) that contribute to XCO_2, which hinders causal attribution of XCO_2 changes to surface anomalies. Monthly anomalies of XCO_2 can thus be more directly attributed to surface carbon flux anomalies than their raw variations can. However, we also evaluate raw XCO_2 enhancements for comparison.

The ΔXCO_2 estimated surface fluxes from Eq. 1 were compared with independently determined surface fluxes using the mean bias, root mean square difference (RMSD), and Pearson's correlation coefficient. Two comparisons were performed: one in a reanalysis framework and another testing OCO-2 observations. In the CarbonTracker reanalysis tests, the surface fluxes were

https://doi.org/10.5194/acp-2022-506
Preprint. Discussion started: 4 August 2022
© Author(s) 2022. CC BY 4.0 License.

Atmospheric Chemistry and Physics Discussions

estimated from CarbonTracker-output XCO_2, wind velocity, and surface pressure using Eq. 1 and were compared against CarbonTracker-output surface CO_2 fluxes, which represent the total surface CO_2 flux from both natural and anthropogenic sources. In the observational assessment, OCO-2 XCO_2 is used to estimate surface CO_2 fluxes along with MERRA2 boundary layer wind velocity and surface pressure in Eq. 1. These XCO_2-based surface CO_2 flux estimates are compared to total surface CO_2 fluxes, which were estimated using the sum of LPJ NBP model anomalies, QFED biomass burning anomalies, and CarbonMonitor fossil fuel estimates. Though CarbonMonitor is only available over a short record, we used the record to determine that the proportion of anthropogenic flux anomalies in the Western US contribute less than 5% to the surface anomalies (see Fig. S1). Therefore, we define total flux estimates of CO_2 in the observation-based assessment to be the sum of LPJ NBP and QFED biomass burning anomalies, acknowledging that there may be additional smaller deviations due to fossil fuel emissions. By varying the target domain region size, these statistics were used to determine the optimal target region size in the Western US, which is sensitive to errors due to atmospheric mixing. This test ultimately determines whether atmospheric mixing over monthly timescales confounds the use of Eq. 1. These statistics were additionally used to assess the optimal wind speed and direction conditions for use of Eq. 1. Namely, these statistics were computed conditioning on ventilation wind speed and direction. Such wind conditions are highly important to assess in such pixel source mass balance methods (Varon et al., 2018).

XCO_2 anomalies and anomaly enhancements were additionally correlated directly with the surface fluxes to determine the degree of surface and atmospheric CO_2 coupling. Specifically, OCO-2 XCO_2 are correlated with the biosphere-only LPJ NBP and FluxSat GPP anomalies to determine how coupled XCO_2 anomalies are to biospheric fluxes at monthly timescales.

OCO-2-retrieved XCO_2's ability to detect the largest surface CO_2 fluxes in the Western US is evaluated using:

$$Detection\ Rate_{x,y} = \frac{N_{\Delta XCO_2>yth\ \&\ Q>xth} + N_{\Delta XCO_2<(1-yth)\ \&\ Q<(1-xth)}}{N_{\Delta XCO_2>yth} + N_{\Delta XCO_2<(1-yth)}} * 100 \quad (2)$$

The detection rate is the percentage of months XCO_2 anomaly enhancements (ΔXCO_2) of a specified magnitude detect surface CO_2 fluxes (Q) of a given magnitude. x is the percentile referring to monthly surface CO_2 flux anomalies and y is the percentile referring to corresponding monthly XCO_2 anomaly enhancements. N is a count of number of Western US domain-averaged pairs that satisfy the conditions in Eq. 2. For example, if x is 75 and y is 95, then the detection rate determines the number of XCO_2 anomaly enhancements above the 95th percentile that are coincident with a surface CO_2 flux anomaly of 75th percentile or above. Eq. 2 also considers the carbon uptake cases of negative XCO_2 anomaly enhancements below the 5th percentile that coincide with a negative surface CO_2 flux anomaly of 25th percentile or less. We use a convention of positive surface CO_2 fluxes being away from the ground. As a property of the detection rate metric, when conditioning on only data pairs when XCO_2 anomaly enhancements are above the 95th percentile (y=95), the detection rate will decrease as the x percentiles are increased. This metric ultimately provides a measure of information that a given XCO_2 anomaly enhancement holds about a corresponding surface CO_2 flux anomaly. This detection rate was compared to detection rates by chance, which are equal to

https://doi.org/10.5194/acp-2022-506
Preprint. Discussion started: 4 August 2022
© Author(s) 2022. CC BY 4.0 License.

Atmospheric Chemistry and Physics Discussions

100-x. We also alternatively evaluated whether the largest surface CO_2 efflux anomalies influence the XCO_2 anomaly signal by estimating the percentage of largest surface efflux anomalies that XCO_2 observes a positive anomaly. We evaluate this metric in several global regions using OCO-2 XCO_2 anomalies and FluxSat GPP to determine whether XCO_2 anomalies can rapidly detect large surface biosphere CO_2 fluxes from extreme events.

Performance of these methods using the observation-based method was compared directly to the CarbonTracker simulation performance, with CarbonTracker tests serving as a "potential" or upper bound on performance given expected XCO_2 observation error from OCO-2.

2.5 XCO_2 Surface Flux Error Estimation

Given known limitations of potentially restrictive greenhouse gas satellite measurement and retrieval errors (Buchwitz et al., 2021), we estimated the effect of these XCO_2 errors on carbon flux estimates, especially their impact on ΔXCO_2. OCO-2 XCO_2 error standard deviation is typically 0.6 ppm for a given observation. However, subtracting two XCO_2 errors and spatial averaging in our procedure in Eq. 1 will have competing amplification and reduction effects on the error standard deviation of ΔXCO_2. Therefore, we estimated the spatially averaged ΔXCO_2 error standard deviation. First, we used a bootstrapping approach to assess subtracting a pair of two XCO_2 errors drawn randomly from a normal distribution with mean zero and 0.6 ppm standard deviation. Errors are assumed to be normally distributed, which is a general property (i.e., central limit theorem) arising from addition of independent, identically distributed satellite instrument errors. Second, we evaluated the response of the error estimate to averaging approximately twenty values (the typical number of soundings in each month in the target Western US domain), which provides a spatially averaged XCO_2 error for both the target and background regions before subtracting the two values. Third, we investigated the role of positive spatial autocorrelation of errors on the overall XCO_2 error standard deviation, where autocorrelation can cause competing effects on XCO_2 anomaly enhancement errors. Namely, if the errors are positively spatially autocorrelated within a given area, noise reduction from spatial averaging will be partially prevented. However, a spatially autocorrelated relationship between XCO_2 errors of the adjacent target and background regions will reduce ΔXCO_2 errors because the XCO_2 errors in the two regions would be positively related.

3 Results and Discussion

3.1 Advection Condition Assessment

Given that we wish to use XCO_2 anomalies in the Western US with only a simple source pixel mass balance method and not an atmospheric transport model and/or assimilation framework to monitor surface CO_2 fluxes, an understanding of the existing advection conditions in the selected domain is critical. Therefore, we first assessed the boundary layer advection conditions (Fig. 1). Eq. 1 was previously applied to smaller spatiotemporal scales (within a kilometer) to estimate emissions of spatially

https://doi.org/10.5194/acp-2022-506
Preprint. Discussion started: 4 August 2022
© Author(s) 2022. CC BY 4.0 License.

Atmospheric Chemistry and Physics Discussions

heterogeneous natural or urban methane plumes (Pandey et al., 2021). However, CO_2 generally has more spatially homogenous surface sources and sinks. Furthermore, we wish to evaluate fluxes from terrestrial ecosystems that exceed tens of kilometers in spatial scales. The need for larger areas and at the monthly aggregated scales thus includes consideration of more atmospheric mixing of widespread CO_2 surface sources and sinks.

As such, it is necessary to understand the advection conditions needed to apply Eq. 1 over large spatial scales, at monthly timescales, and for CO_2 that has more spatially distributed surface contributions than CH_4. Under these considerations, the most ideal conditions for Eq. 1 appear to be winds that, on average over a month, consistently originate from a single background region and flow steadily and consistently (without greatly changing directions) through the region throughout the year. These conditions typically hold in the Western US where winds originate from the Pacific Ocean and flow west to east consistently through the domain (Fig. 1). By contrast, the advection conditions may be more complex in a region like the Southeast US which experiences changes in background source of incoming advection from the Midwestern US in the fall and winter to the Gulf of Mexico in the spring and summer. These variable background conditions and inconsistent wind directions may create large errors when applying Eq. 1.

A more comprehensive evaluation of the boundary layer wind vectors reveals that the Pacific Ocean at the region's west border comprises the main source of advection entering the target region throughout the year (Fig. 2a). Winds along its northern, southern, and eastern borders have little contribution to the region. This suggests that Eq. 1 can be applied more confidently in assuming only one background region contributes advection to the Western US. More detailed evaluation of the incoming advection from the Pacific Ocean reveals that incoming winds at the western border and throughout the region are continuously of non-negligible magnitude and consistently to the east (Figs. 2b and 2c). The exception is spring and summer months when winds in the Pacific Ocean shift to the south and the speed of eastward winds into and within the region are lower.

Nevertheless, these conditions initially indicate that the Western US region is a candidate region to detect and estimate surface fluxes using satellite XCO_2 retrievals. We test the ability to estimate surface CO_2 fluxes from XCO_2 under these advection conditions using CarbonTracker reanalysis hereafter.

https://doi.org/10.5194/acp-2022-506
Preprint. Discussion started: 4 August 2022
© Author(s) 2022. CC BY 4.0 License.

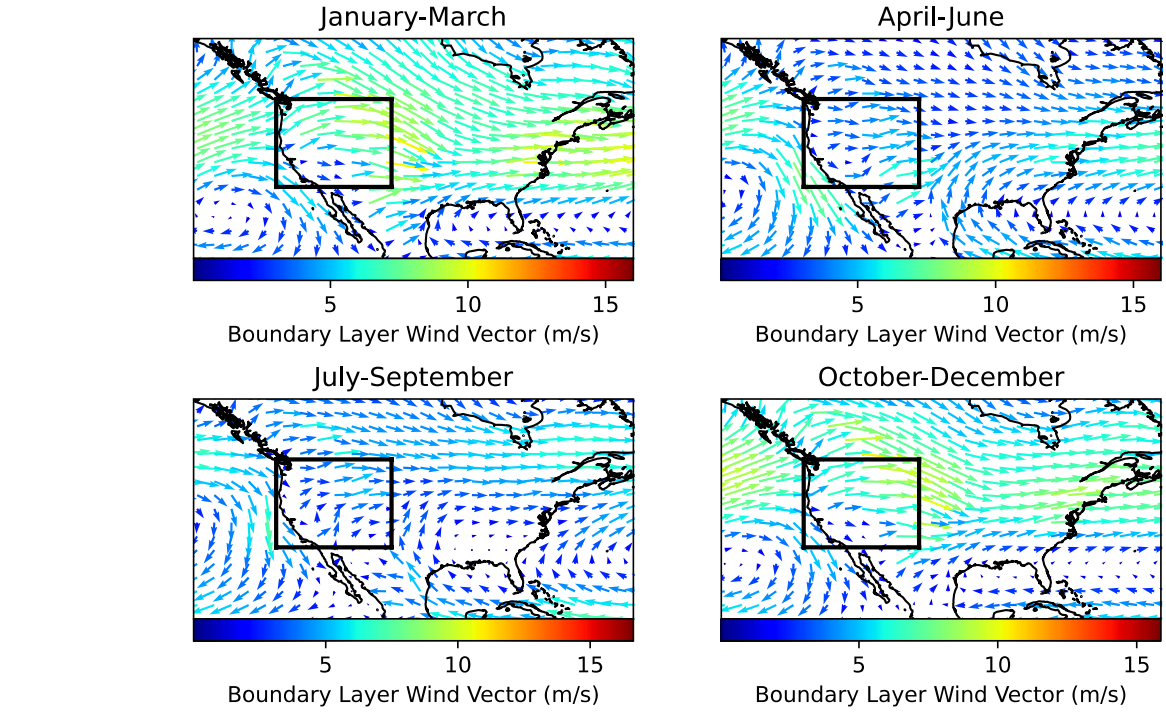

Figure 1. Mean monthly boundary layer (surface up to approximately 700 mb) conditions from MERRA2 in each season. The Western US target domain is identified with borders.

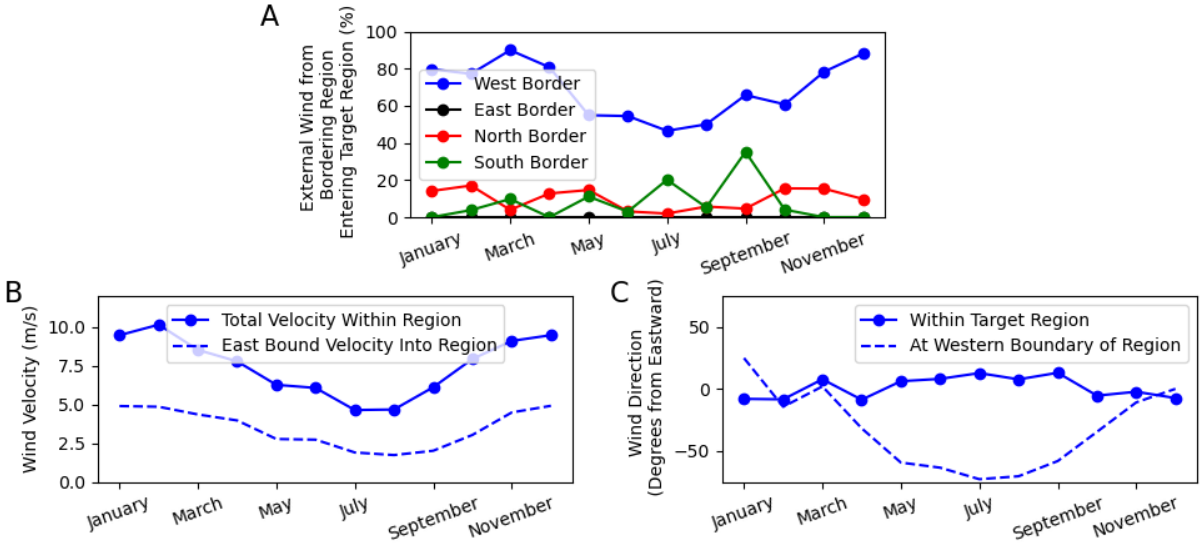

Figure 2. Mean monthly advection conditions in the Western US target domain in Fig. 1. **(a)** Proportion of wind vector entering region from each bordering region. Values do not add to 100% because each border's wind vector is evaluated individually for its contribution to the

https://doi.org/10.5194/acp-2022-506
Preprint. Discussion started: 4 August 2022
© Author(s) 2022. CC BY 4.0 License.

Atmospheric Chemistry and Physics Discussions

Western US domain. **(b)** Mean wind velocity and **(c)** mean wind direction within the target region and eastward into the target domain from the Pacific Ocean on its western border.

3.2 Reanalysis Evaluation

Here, using CarbonTracker (CT2019B) model reanalysis as a testbed, we evaluate by how much the advection conditions present limitations for detecting and estimating surface CO_2 fluxes using XCO_2 anomalies in the Western US. We tested the effect of domain area size, wind angle, and wind speed on the mass balance surface flux estimation.

Using CarbonTracker, we find that a smaller target region has a large decline in ability to estimate surface fluxes with Eq. 1 (Fig. 3). This reduction in performance of the simple mass balance model is expected because a smaller area will increase importance of turbulent mixing compared to effects of mean horizontal ventilation wind, as was suggested previously (Varon et al., 2018). It will also include XCO_2 contributions from surface sources outside of the selected target region due to mixing. For example, with turbulent mixing on smaller spatial scales, large CO_2 surface effluxes from surfaces adjacent to the region may mix with atmospheric CO_2 within the region, causing a larger positive XCO_2 anomaly than what can be expected from the surface contributions from within the small target domain itself. In fact, the increasing positive mean bias with smaller selected target areas suggests this may be the case where XCO_2 within the target region includes contributions from more surface area than the mass balance model can predict (Fig. 3c). The decorrelation of the XCO_2 surface flux estimates with the modeled surface fluxes with smaller surface areas further supports this claim where external XCO_2 anomaly variations may be effectively contributing to the XCO_2 anomalies within the domain (Fig. 3a). Ultimately, this target region size analysis motivates choosing larger target areas for application of Eq. 1 on CO_2 flux estimation, especially over monthly timescales.

In the context of this application for studying the terrestrial biosphere, we speculate that choosing larger regional domains creates greater requirements on the need for consistent advection conditions over a larger spatial scale, limiting the number of areas of the globe where such a method can be applied. If boundary layer winds tend to change directions within the domain or originate from multiple background regions, a smaller domain may simplify the conditions for use of Eq. 1. However, the choice of a smaller area will have competing effects of an increased error due to mixing and turbulence as suggested by Fig. 3 and previous work (Varon et al., 2018). As such, in cases of more complex advection conditions, regions the size of that in Fig. 3e may be optimal.

While variations in the monthly averaged wind speed through the Western US (typically ranging from 1 m/s to 10 m/s) does not consistently impact XCO_2 surface flux estimation, large deviations in wind angle from the eastward direction incoming from the Pacific Ocean can negatively impact flux estimation (Fig. 4). Namely, there is a general reduction in the mass balance equation's (Eq. 1) ability to estimate surface fluxes with increasing wind angle (Fig. 4a). While absolute errors only weakly linearly increase with wind angle ($r = 0.12$; p-value=0.07) (RMSD's correlation with wind angle is $r = 0.53$, p-value = 0.16

https://doi.org/10.5194/acp-2022-506
Preprint. Discussion started: 4 August 2022
© Author(s) 2022. CC BY 4.0 License.

Atmospheric Chemistry and Physics Discussions

with only eight bin samples), a more frequent occurrence of higher errors occurs above absolute angles of 60 degrees from the eastward plane (Fig. 4a). As such, the switch to northerly winds in the Pacific Ocean during the summer months (Fig. 2c) may the cause of seasonally increased surface CO_2 flux estimation errors (Fig. 4c). This is expected because the advection of air from the Pacific Ocean into the Western US would be reduced, creating a disconnect between the atmospheric carbon concentrations of the Western US target region and Pacific Ocean in these months (Fig. 1). The effect of variations in monthly averaged wind speed appears to have less of an influence on errors than wind angle (Fig. 4b). Specifically, there is a correlation of 0.02 (p-value=0.7) between wind speed and absolute errors. However, we expect errors would increase if wind speeds approach zero. Wind speed may also become a larger error source when investigating shorter time steps or more spatially heterogeneous anthropogenic plumes (Jacob et al., 2016; Varon et al., 2018).

Overall, the simple mass balance estimation of surface fluxes with XCO_2 (Eq. 1) appears robust to the range of advection conditions in the Western US, except potentially for summer months when Pacific Ocean winds can shift from westerlies to northerlies (Fig. 5). XCO_2 anomaly enhancements are positively correlated with surface flux anomalies in the Western US, especially in cases when the wind angle has a non-negligible eastward component (Fig. 5a). This correlation is maintained when applying Eq. 1 to estimate surface fluxes (Fig. 5b). The comparison improves when consideration of winds that have a wind angle from the eastward reference of less than 60 degrees, or between -60 and 60 degrees when 0 degrees is to the east (Fig. 5). However, we caution that an RMSD of ~20 TgC per month suggests that the approach should be used only as a rapid, first estimation of surface CO_2 flux anomalies.

We additionally show that the method can estimate the surface CO_2 fluxes using the raw XCO_2 enhancements (i.e., not anomalies), especially when winds have a substantial eastward component (Fig. 5c). However, using the XCO_2 anomalies removes seasonal XCO_2 enhancement variability that may not be attributed to surface fluxes, which collapses the data pairs more along the 1:1 line (compare Figs. 5b and 5c).

Therefore, our tests with CarbonTracker model reanalysis reveal that XCO_2 can indeed be used to viably estimate monthly surface CO_2 fluxes with simple mass balance approaches, especially over spatial extents of natural ecosystems. However, the method requires favorable conditions mainly related to advection. Namely, the region size must be large enough to account for atmospheric mixing that could dominate transport in smaller domains over monthly timescales. Additionally, based on Figures 4 and 5 and assumptions of the mass balance model, winds must flow consistently through the region with a similar direction. Given the need for XCO_2 enhancements, the transport should originate from the same background source region within a given month rather than from multiple background regions. We speculate that the method may additionally work well in the Western US given the upwind Pacific Ocean region tends to have low anthropogenic sources and relatively lower CO_2 surface emissions and anomalies altogether. Thus, the XCO_2 enhancement variability will likely not be dominated by the background region's XCO_2 variability.

https://doi.org/10.5194/acp-2022-506
Preprint. Discussion started: 4 August 2022
© Author(s) 2022. CC BY 4.0 License.

Atmospheric Chemistry and Physics Discussions

While the simple mass balance approach appears suitable for use based on a model reanalysis framework, repeating the procedure with observations such as with OCO-2 presents additional challenges, such as with observation error and spatiotemporal coverage. As such, CarbonTracker performance here effectively serves as an upper bound on predicting XCO_2's ability to be coupled to surface CO_2 fluxes, acknowledging modeling sources of error. We address these issues in the following section.

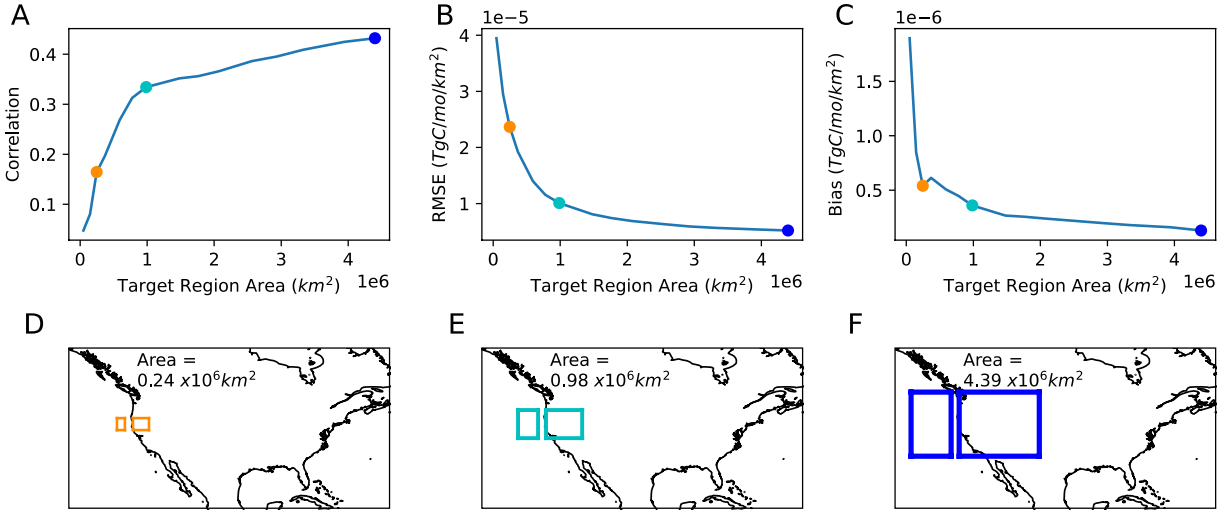

Figure 3. Performance of the XCO_2-based CO_2 flux estimation varying the target domain area. **(a)** Correlation, **(b)** root mean square error, and **(c)** bias between the CarbonTracker monthly surface flux anomaly outputs (considered here as the reference) and the CO_2 flux anomaly estimation with Eq. 1 based on XCO_2 from CarbonTracker. **(d, e, f)** Target domain sizes and locations where their domain border colors match the dot symbol colors in panels A-C.

https://doi.org/10.5194/acp-2022-506
Preprint. Discussion started: 4 August 2022
© Author(s) 2022. CC BY 4.0 License.

Atmospheric Chemistry and Physics Discussions

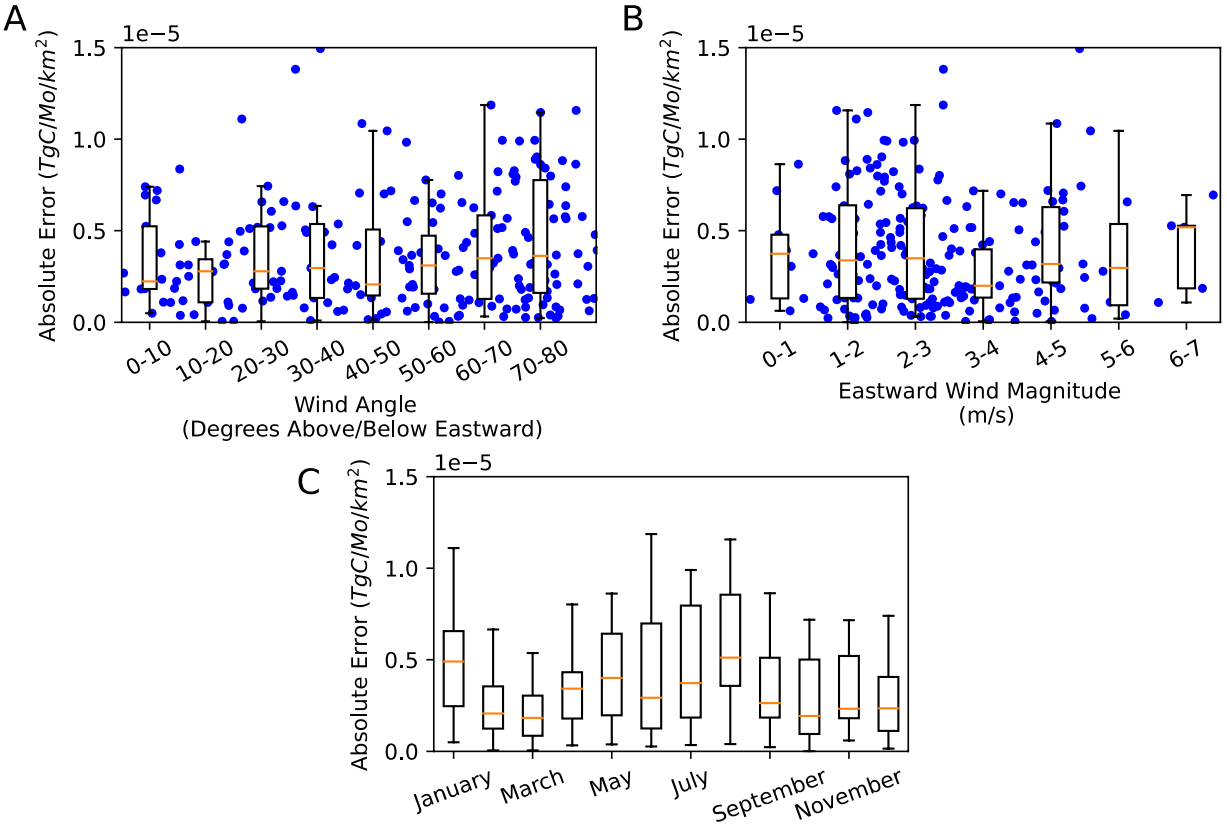

400

Figure 4. Effect of monthly averaged horizontal ventilation wind conditions on carbon flux anomaly estimation using CarbonTracker outputs. Carbon flux anomaly estimation error with respect to boundary layer **(a)** wind angle and **(b)** wind speed. **(c)** Carbon flux anomaly estimation error averaged over each month of year. Absolute error is the absolute value of the difference between each pair of CarbonTracker XCO_2 flux estimates using Eq. 1 and CarbonTracker surface CO_2 flux outputs.

https://doi.org/10.5194/acp-2022-506
Preprint. Discussion started: 4 August 2022
© Author(s) 2022. CC BY 4.0 License.

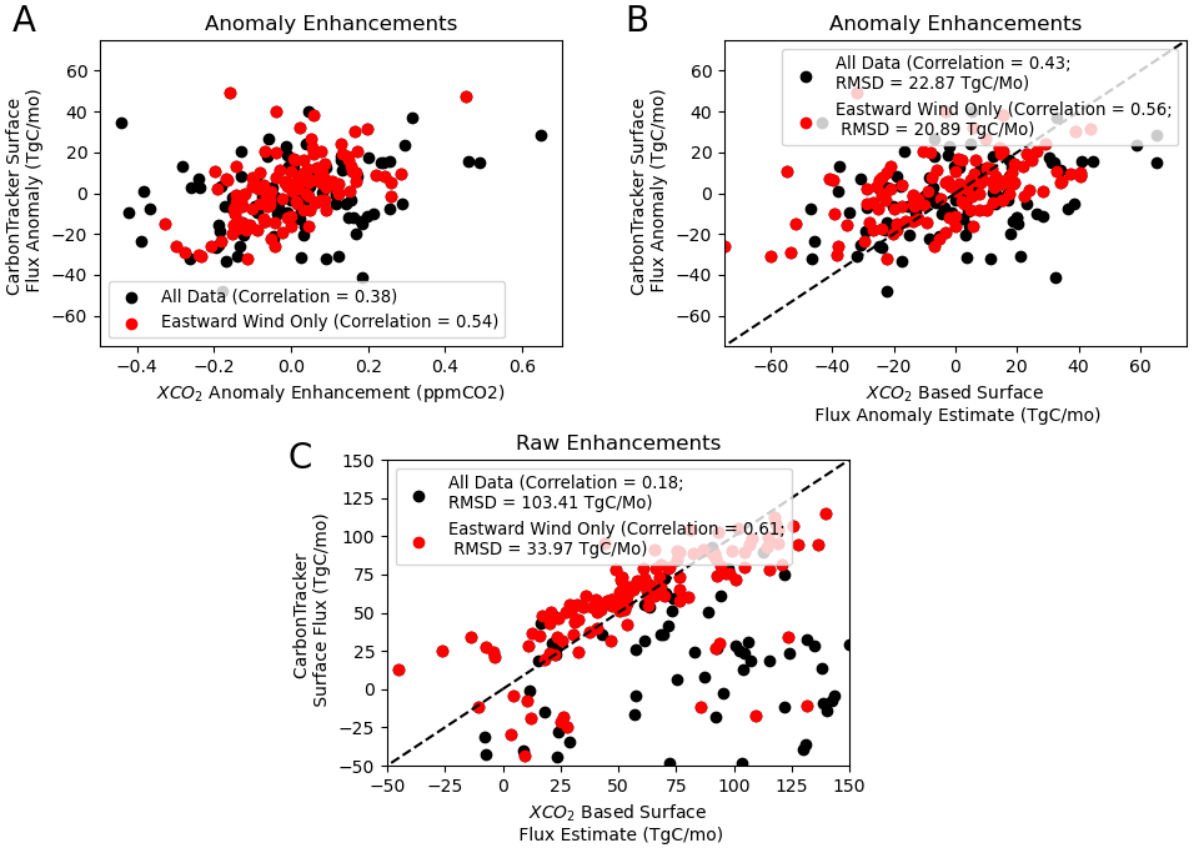

Figure 5. CarbonTracker XCO_2 flux estimation overall performance in the Western US considering a spatially expansive target domain (latitude = 33° N - 49° N, longitude = 124° W - 104° W as shown in Fig. 3f). Only CarbonTracker data was used here where its XCO_2, wind velocity, and pressure outputs were used to estimate surface CO_2 fluxes with Eq. 1, which are compared to CarbonTracker total surface CO_2 flux outputs. **(a)** Relationship between CarbonTracker-output surface CO_2 flux anomalies and CarbonTracker XCO_2 anomaly enhancements. **(b)** Relationship between CarbonTracker surface CO_2 flux anomaly outputs and mass balance-based surface CO_2 flux estimates based on CarbonTracker XCO_2 anomaly enhancements. **(c)** Same as **(b)** but estimating raw total surface fluxes with total XCO_2 enhancements instead of anomalies. Legends show correlations and root mean square differences between the CarbonTracker XCO_2-based flux estimates (Eq. 1) and CarbonTracker surface CO_2 flux outputs. "Eastward Wind Only" includes only data pairs when the incoming wind direction from the Pacific Ocean is between -60° and 60° angles from eastward reference direction.

3.3 Observations Evaluation

3.3.1 OCO-2 XCO_2 Anomaly Coupling to Surface CO_2 Fluxes

OCO-2 XCO_2 anomalies are coupled to biospheric flux anomalies in the Western US region as expected from the CarbonTracker analysis in Sect. 3.2 (Fig. 6). XCO_2 anomalies negatively correlate with land surface model simulated net biome production and satellite-derived gross primary production anomalies, especially in the Western US domain (Fig. 6). For

https://doi.org/10.5194/acp-2022-506
Preprint. Discussion started: 4 August 2022
© Author(s) 2022. CC BY 4.0 License.

Atmospheric Chemistry and Physics Discussions

example, monthly carbon uptake from increases in NBP and GPP are coincident with decreases in XCO_2 and vice versa. Their coupling is less consistent and reduced in the East US, presumably due to less ideal advection conditions where transport anomalies confound direct surface-atmosphere CO_2 coupling. Nevertheless, the Western US surface-atmosphere CO_2 coupling appears weaker than that shown in Fig. 5, which may be due to several additional sources of error that we investigate in Sect. 3.3.2.

The fact that spatially averaged XCO_2 anomalies are coupled to surface fluxes (Fig. 7) suggests that observed XCO_2 shows promise for directly detecting and estimating large-scale biospheric surface fluxes without the use of land surface and atmospheric transport assimilation models. The XCO_2 coupling to land surface carbon fluxes tends to increase when Pacific Ocean background XCO_2 are subtracted from Western US XCO_2 (Fig. 7a) (i.e., when XCO_2 anomaly enhancements are used). The coupling further increases when only months with eastward flowing winds into the region are considered, at least for the total flux estimates (Fig. 7a). Such increased coupling accounting for advection in this way is expected from the CarbonTracker model reanalysis tests (Fig. 5a). This is because XCO_2 anomalies coupling with surface CO_2 fluxes are confounded by XCO_2 change due to transport conditions. For example, many Western US XCO_2 anomalies appear correlated to Pacific Ocean background XCO_2 anomalies in 2015 to 2016 suggesting that Western US XCO_2 variations were dominated by atmospheric transport rather than surface fluxes in this time period (Fig. 7c). Therefore, XCO_2 anomaly enhancements can increase this coupling to the surface CO_2 fluxes by removing the confounding variations of background Pacific Ocean CO_2 concentrations transported into the region (Fig. 7d). However, some large anomaly enhancements may occur in months that advection was not consistently flowing through the region, thus requiring conditioning on wind angles. This removes cases of large XCO_2 differences between the two regions that may not necessarily be enhancements because atmospheric transport between these two regions was reduced in these months (examples can be seen in late 2017 in Figs. 7c and 7d).

Even after isolating the effects of background Pacific Ocean XCO_2 and abnormal advection conditions, the magnitude of these observation-based correlations of 0.32 (Fig. 7a) are lower than that of CarbonTracker reanalysis tests at a correlation of 0.54 (Fig. 5a). Indeed, the total fluxes are estimated by LPJ NBP and QFED burning biomass which include model estimations and assumptions with their own sets of errors. However, the surface-atmosphere carbon coupling is similar considering only photosynthesis fluxes from independently estimated GPP (Fig. 7a), which suggests a large role of the biosphere on the carbon fluxes and that LPJ model error may not be the main contribution to the correlation reduction. We ultimately expect that a main source of reduction in coupling originates from OCO-2 measurement and retrieval error.

https://doi.org/10.5194/acp-2022-506
Preprint. Discussion started: 4 August 2022
© Author(s) 2022. CC BY 4.0 License.

Atmospheric Chemistry and Physics Discussions

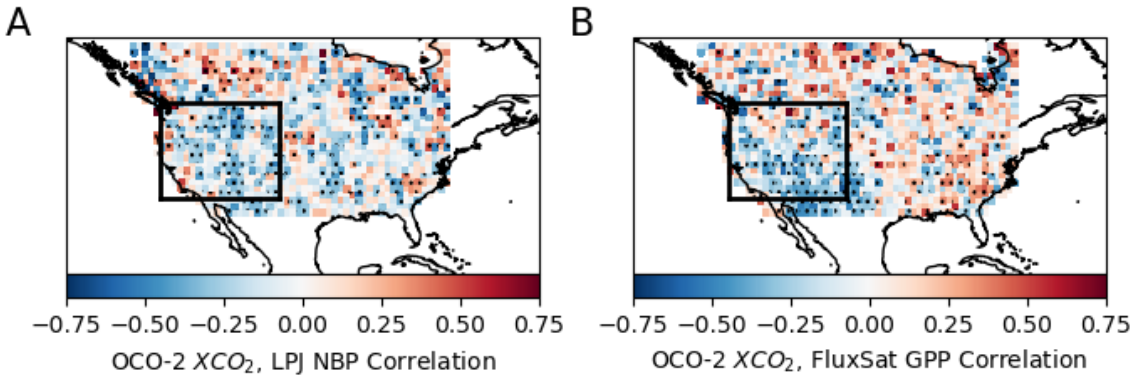

Figure 6. Observed OCO-2 XCO_2 anomalies are correlated with independent biospheric surface fluxes in Western US (with no time lag). **(a)** Correlation between OCO-2 XCO_2 anomalies and LPJ modeled net biome production anomalies. **(b)** Correlation between OCO-2 XCO_2 anomalies and observation-based FluxSat gross primary production anomalies. Negative correlations indicate that XCO_2 anomalies are coupled with the biospheric surface anomalies (i.e., increases in biosphere carbon uptake result in decreases in XCO_2). Pixels with stippling indicate p values less than 0.1.

https://doi.org/10.5194/acp-2022-506
Preprint. Discussion started: 4 August 2022
© Author(s) 2022. CC BY 4.0 License.

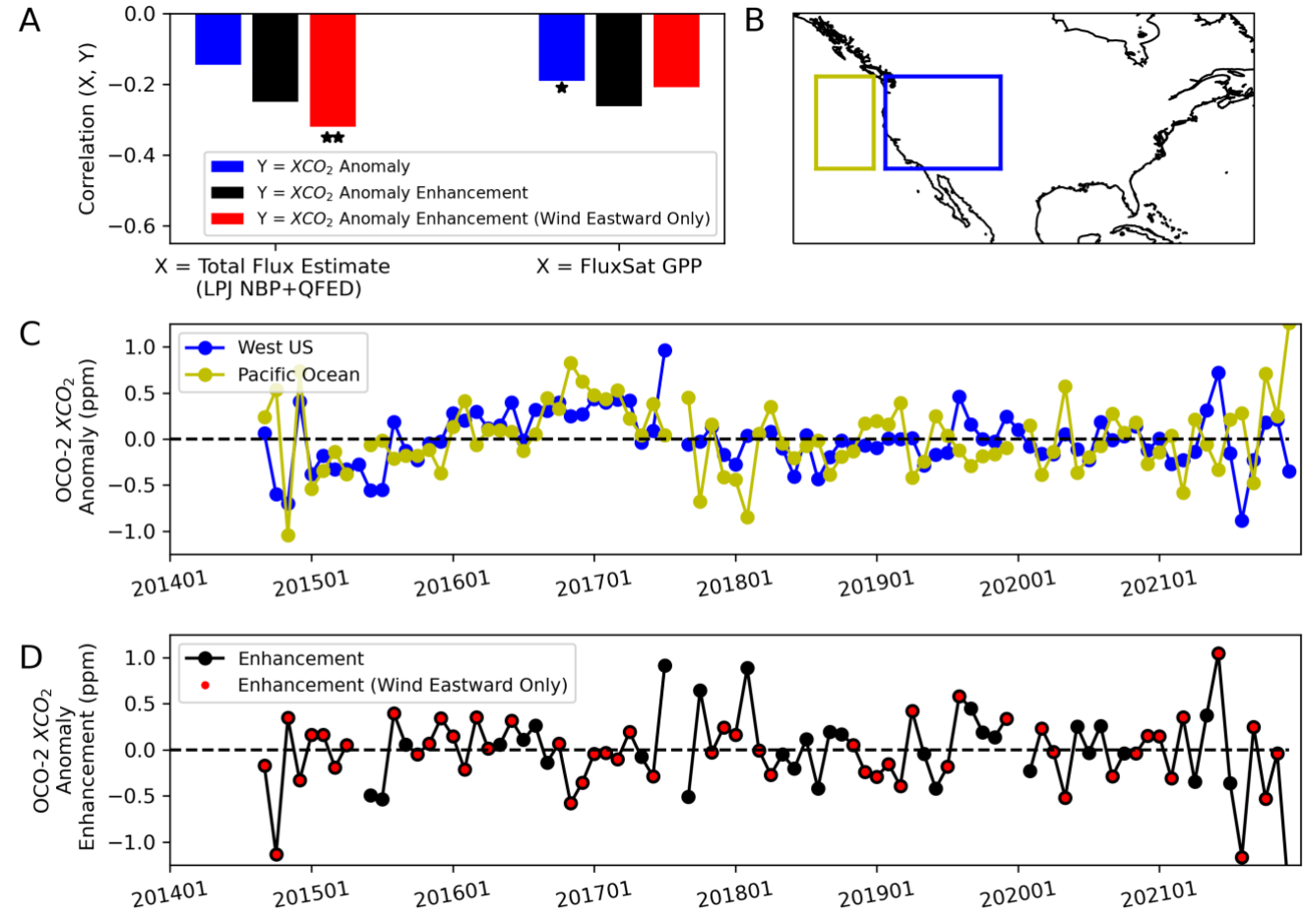

Figure 7. (a) Pearson correlation coefficients between the XCO_2 anomalies and total surface CO_2 flux estimates (LPJ model and QFED biomass burning) as well as with observation-based FluxSat (** p-value<0.05; * p-value<0.1). **(b)** Map of Western US and background Pacific Ocean background domain definitions. **(c)** Spatially averaged OCO-2 XCO_2 anomalies in the Western US and background Pacific Ocean. **(d)** Western US XCO_2 anomaly enhancements from the background Pacific Ocean OCO-2 XCO_2 anomalies. Red symbols are months when the incoming wind direction from the Pacific Ocean was between -60° and 60° angles from eastward reference direction.

3.3.2 Error Estimation of XCO_2 Anomaly Enhancements

While subtracting a pair of XCO_2 anomalies to obtain anomaly enhancements increases errors above that of individual OCO-2 XCO_2 retrievals, spatial averaging of XCO_2 across a large domain reduces these errors (Fig. 8). OCO-2 XCO_2 error standard deviations for individual sounding retrievals are estimated to be 0.6 ppm in the Western US and 0.55 ppm in the Pacific Ocean. This results in an error standard deviation of approximately 0.82 ppm for XCO_2 anomaly enhancements (or difference between a pair of XCO_2 retrievals between the Western US and Pacific Ocean) (Fig. 8a). However, assuming normally distributed and independent errors, spatial averaging of approximately 20 observations within the Western US target region and 10

https://doi.org/10.5194/acp-2022-506
Preprint. Discussion started: 4 August 2022
© Author(s) 2022. CC BY 4.0 License.

Atmospheric Chemistry and Physics Discussions

observations in the Pacific Ocean background region (typical OCO-2 observation counts in the study region in Fig. 7B) reduces this error standard deviation of Western US XCO_2 anomaly enhancements to around 0.2 ppm (Fig. 8b). This error magnitude is similar to that found in Chatterjee et al. (2017) when averaging over monthly timescales over a region. We find that spatial autocorrelation of errors (relaxing assumption of independent errors) may not greatly change this error standard deviation due to competing effects (Fig. 8c). Specifically, spatial autocorrelation of errors removes some noise reduction benefits when averaging within a region due to a spatial relationship between the errors, rather than random errors. However, this spatial relationship in errors also results in a partial canceling of errors when subtracting the spatially averaged Western US XCO_2 anomaly error from the spatially averaged Pacific Ocean XCO_2 anomaly error to obtain XCO_2 anomaly enhancements. Ultimately, a given month's XCO_2 anomaly enhancement in our Western US target region is about 0.2 ppm, or a third of that of a single XCO_2 retrieval's error. Therefore, aggregating XCO_2 anomalies and enhancements spatially and temporally may allow detection of smaller XCO_2 anomalies given that the emission source anomalies themselves are on the order of the spatial and temporal aggregation.

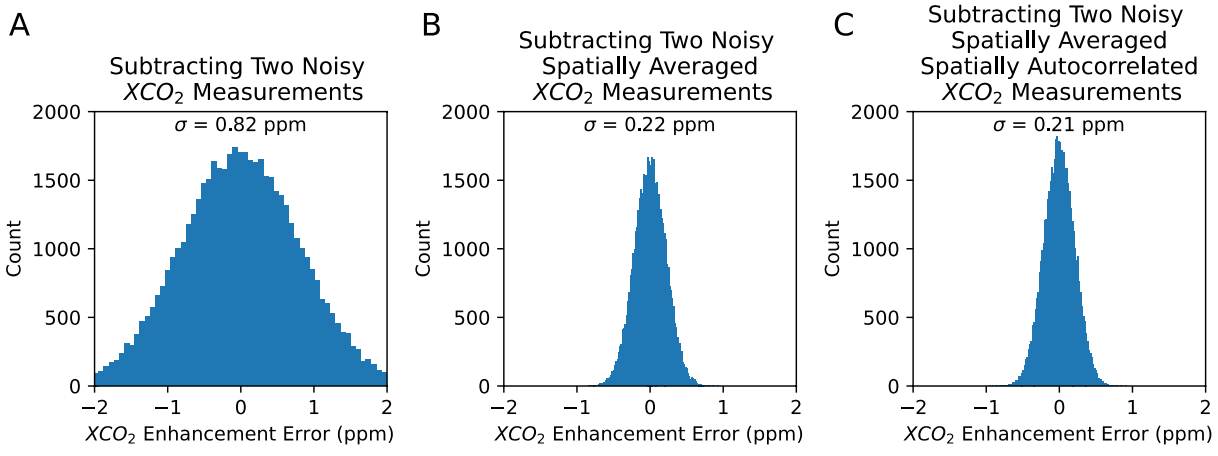

Figure 8. XCO_2 enhancement error based on subtracting two noisy, spatially averaged XCO_2 retrievals using simulated additions of random XCO_2 error. For a given sounding, OCO-2 XCO_2 retrieval error is on average 0.6 ppm in the West U.S. and 0.55 ppm in the Pacific Ocean. **(a)** XCO_2 enhancement error considering subtracting two independent, noisy measurements. **(b)** XCO_2 enhancement error considering the spatial averaging of XCO_2 retrievals in the target and background regions, with all errors assumed to be independent. **(c)** XCO_2 enhancement error considering the spatial averaging of XCO_2 retrievals in the target and background regions, but assuming errors are spatially autocorrelated within each region and spatially autocorrelated between the background and target region.

3.3.3 OCO-2 XCO_2 Estimation of Monthly Surface CO_2 Fluxes

Carbon flux anomaly estimates from OCO-2 XCO_2 using Eq. 1 weakly co-vary with modeled and observation-based surface CO_2 flux anomalies (Fig. 9). In general, the simple mass balance method increases its ability to estimate surface CO_2 fluxes when conditioning on the "best" atmospheric transport conditions as shown across correlation, mean bias, and RMSD statistics

https://doi.org/10.5194/acp-2022-506
Preprint. Discussion started: 4 August 2022
© Author(s) 2022. CC BY 4.0 License.

Atmospheric Chemistry and Physics Discussions

(Fig. 9). However, the performance of the flux estimation method is reduced overall when using OCO-2 observations compared to CarbonTracker model reanalysis tests (shown for comparison in Fig. 9).

Even though spatial averaging reduces observation error of XCO_2 anomaly enhancements, we show that reduced simple mass balance flux estimation performance can largely be attributed to OCO-2 XCO_2 retrieval errors (from OCO-2 instrument measurement error and algorithmic retrieval error). Specifically, adding this approximate 0.2 ppm error randomly to CarbonTracker XCO_2 outputs results in comparison statistics that approach that based on observed OCO-2 (see Figs. 9b to 9d especially for correlation and RMSD). Other error sources likely also explain the reduced comparison between OCO-2-based estimates and surface modeled estimates including MERRA2 wind vector error, reference surface flux error (from LPJ biosphere model and QFED fire estimate error), inconsistent XCO_2 spatiotemporal coverage within each region, and Eq. 1 mass balance model errors. However, our test reveals that greenhouse gas satellite retrieval error is a dominant component of the overall error in estimating surface fluxes. Ultimately, the retrieval error in OCO-2 XCO_2 hinders reliable estimation of nominal monthly surface flux anomalies using rapid mass balance approaches, as expected from simulations (Chevallier et al., 2007). Indeed, more accurate greenhouse-gas satellite missions would be needed to approach the potential surface flux estimation performance with mass balance models as suggested by CarbonTracker reanalysis.

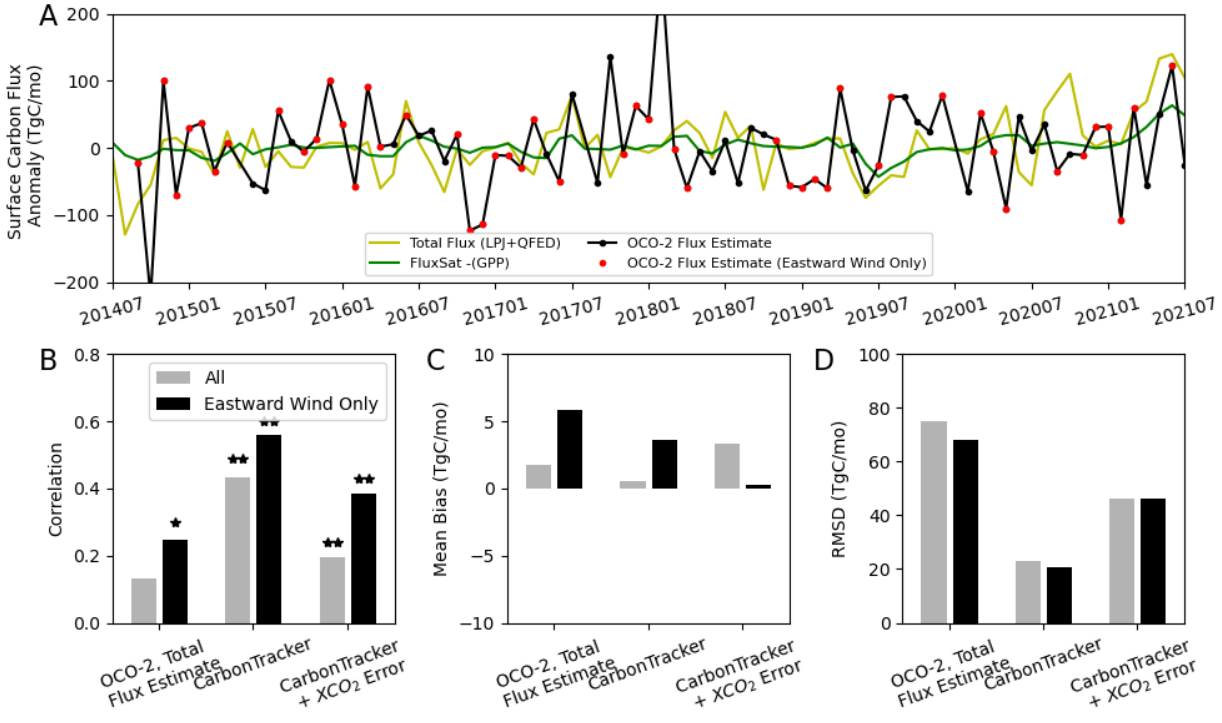

Figure 9. (a) Spatially averaged OCO-2 XCO_2 flux anomaly estimates compared to total flux estimate anomalies (LPJ model and QFED biomass burning) and FluxSat gross primary production anomalies. Positive anomalies are fluxes away from the surface. Comparison

https://doi.org/10.5194/acp-2022-506
Preprint. Discussion started: 4 August 2022
© Author(s) 2022. CC BY 4.0 License.

Atmospheric Chemistry and Physics Discussions

statistics between OCO-2 flux anomaly estimates and LPJ NBP anomalies with **(b)** correlation (** p-value<0.05; * p-value<0.1), **(c)** mean bias, and **(d)** root mean square difference (RMSD). CarbonTracker comparisons are shown for reference repeated from Fig. 5. CarbonTracker+XCO_2 Error includes simulated error added to CarbonTracker modeled XCO_2 on the order of that shown in Fig. 8. The statistics are computed for all data pairs as well as only those considering months when the incoming wind direction from the Pacific Ocean was between -60° and 60° angles from eastward reference direction.

3.3.4 OCO-2 XCO_2 Detection and Estimation of Extreme Surface CO_2 Fluxes

Although OCO-2 measurement noise limits estimation of smaller monthly surface flux anomalies using XCO_2, OCO-2 XCO_2 retrievals show promise in directly detecting and estimating the largest surface CO_2 flux anomalies. Despite OCO-2 noise levels (of 0.2 ppm to 0.6 ppm depending on averaging of individual soundings), large XCO_2 anomalies above the noise are likely indicative of a large surface flux anomaly in the Western US. This is expected from previous studies that XCO_2 0.5 ppm changes or greater may be detecting a physically-driven atmospheric carbon concentration anomaly (Chatterjee et al., 2017).

To highlight the ability of XCO_2 anomaly enhancements to directly detect extreme carbon cycle events in the Western US, we evaluate the XCO_2 detection rate (Eq. 2) of surface CO_2 anomalies across a range of nominal to extreme conditions (Fig. 10). Figs. 10a to 10C show that when XCO_2 anomaly enhancements are large (>90th percentile), they are frequently detecting above average surface CO_2 flux anomalies for both observation and model assessments. As expected from Figs. 8 and 9, the detection rates are higher in the CarbonTracker reanalysis testbed across all conditions than for observations, likely due to OCO-2 XCO_2 retrieval error considerations. Additionally, as expected from positive correlations between surface CO_2 flux anomalies and XCO_2 anomaly enhancements, larger XCO_2 anomaly enhancements are better able to detect surface CO_2 flux anomalies than smaller XCO_2 anomaly enhancements. Figs. 10d to 10f specifically show the degree to which an XCO_2 anomaly enhancement can detect a given magnitude of surface CO_2 flux anomalies greater than by chance. CarbonTracker XCO_2 anomaly enhancements can detect surface carbon flux anomalies of at least the same percentile well above that by chance in nearly all cases (Fig. 10f). However, OCO-2 XCO_2 anomaly enhancements can only detect surface CO_2 flux anomalies when XCO_2 anomaly enhancements are the largest (>90th percentile), demonstrating how OCO-2 retrieval error largely removes the surface flux information content of a smaller magnitude XCO_2 anomaly (Figs. 10d and 10e). Nevertheless, the largest OCO-2 XCO_2 anomalies enhancements within the Western US are frequently associated with a surface CO_2 flux anomaly.

In the context of terrestrial biosphere extremes (i.e., droughts and heatwaves), we additionally evaluate whether extreme surface CO_2 efflux anomalies create a positive XCO_2 anomaly (Fig. 11). Using OCO-2 XCO_2 anomalies alone (without enhancements), the XCO_2 detection rate of the largest biospheric surface efflux anomalies (>95th percentile) exceeds 50% (Fig. 11). Thus, OCO-2 will detect the surface CO_2 flux signal as a positive XCO_2 anomaly under extreme biosphere conditions, beyond only by chance. OCO-2 XCO_2 anomalies detect 60% of the largest total surface efflux anomalies in the Western US study domain (Fig. 11a). With reduced satellite instrument noise, the detection could increase to 80%, a detection rate potential

https://doi.org/10.5194/acp-2022-506
Preprint. Discussion started: 4 August 2022
© Author(s) 2022. CC BY 4.0 License.

Atmospheric Chemistry and Physics Discussions

estimated from CarbonTracker. When considering photosynthesis anomalies available globally with the MODIS-based FluxSAT GPP dataset, XCO_2 positive anomalies have detected between 60% and 100% of the most extreme negative photosynthesis anomalies across several regions of the world (Fig. 11). These other regions, including the Sahel, Central Europe, and West Australia, were selected given that they have had extreme biospheric anomalies over the past two decades (Fig. 11). In assessing only the XCO_2 anomalies, we are not considering transport conditions, where regions like West Australia have transport conditions less conducive for surface flux estimation with Eq. 1 than the Western US. Nevertheless, when a climatic event is ongoing and model outputs of surface carbon fluxes are not yet available, OCO-2 XCO_2 anomalies can be rapidly consulted. If a large XCO_2 anomalies is detected, it can be used as the motivation to initiate a more detailed investigation and/or monitoring campaign of the climatic event.

We also show that the simple mass balance method (Eq. 1) approximately estimates these extreme fluxes that it detects in the Western US (Fig. 12). The 2021 fluxes in March and June were part of an extreme Western US drought and heatwave event (Philip et al., 2021; Williams et al., 2022). The LPJ model and QFED wildfire estimates indicated that these total efflux anomalies increased to a peak in Spring 2021 (Fig. 9a). In June, the OCO-2-based flux estimate finds a 122 TgC/mo anomaly, while the independent total flux estimate from LPJ and QFED is 140 TgC/mo (Fig. 12). Therefore, the simple mass balance method provides a viable method to rapidly estimate the extreme fluxes from a satellite observation source compared to more complex modeling and reanalysis. In the months when XCO_2-based flux anomalies did not compare with that estimated in 2020, the total flux estimates (from LPJ and QFED) potentially were positively biased when FluxSat GPP did not indicate large biosphere flux anomalies (Fig. 9a). Therefore, the extreme flux estimates from other sources may have had model related errors that resulted in the reduced comparison.

While such a simple mass balance approach does not supplant a rigorous flux assimilation, it serves as a rapid estimation approach that can be used within one to two months latency. This is significant given the typical one-month latency of greenhouse gas satellites like OCO-2, while total surface flux estimates that require biosphere model ensemble implementations are often multi-month or multi-year efforts. As such, greenhouse gas satellites can be consulted for rapid monitoring and attribution to determine whether an ongoing extreme climatic anomaly (i.e, the Western US 2020-2021 drought) is creating substantial carbon cycle anomalies.

https://doi.org/10.5194/acp-2022-506
Preprint. Discussion started: 4 August 2022
© Author(s) 2022. CC BY 4.0 License.

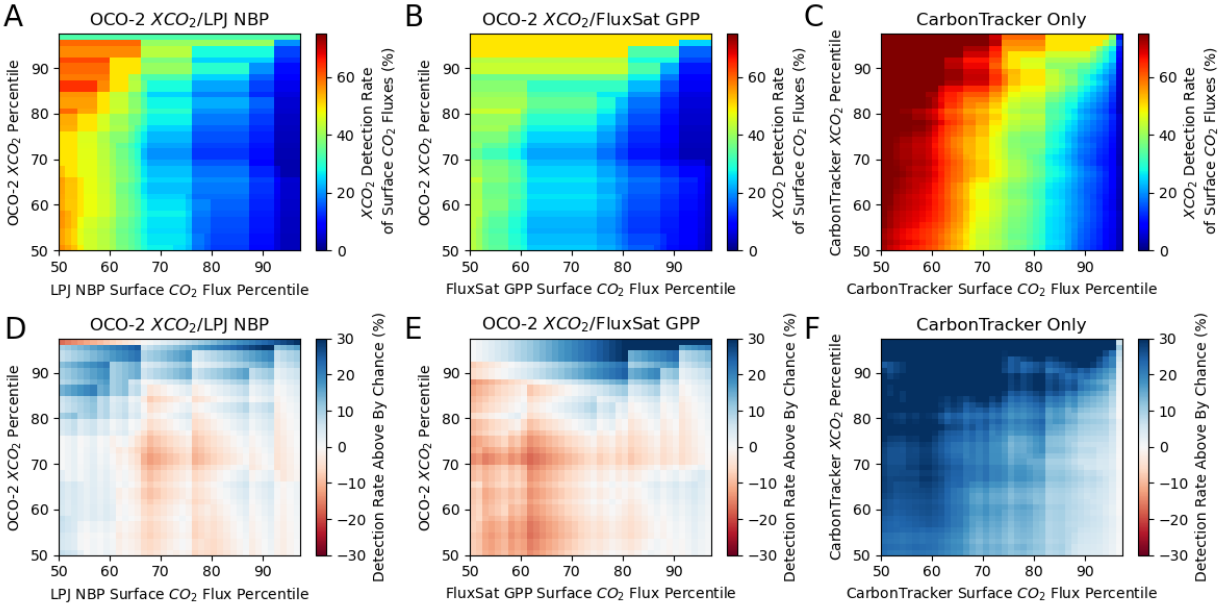

Figure 10. OCO-2-retrieved XCO_2 anomaly enhancements that are more extreme (>90th percentile) can detect surface CO_2 anomalies. By contrast, less extreme retrieved XCO_2 anomaly enhancements (50th-80th percentile) have little ability to detect surface CO_2 anomalies. **(a, b, c)** Western US observed XCO_2 anomaly enhancements detection rate of surface CO_2 fluxes for **(a)** OCO-2 XCO_2 detection of LPJ NBP surface fluxes and **(b)** OCO-2 XCO_2 detection of FluxSat GPP surface fluxes. This is compared to detection rates from the reanalysis testbed in the absence of satellite retrieval error for **(c)** CarbonTracker XCO_2 detection of CarbonTracker CO_2 surface fluxes. Each detection rate value is estimated by binning all XCO_2 anomaly enhancements above the given percentile (y-axis) and determining the number of coincident monthly surface CO_2 flux anomalies that are above the given CO_2 flux percentile (x-axis). Detection rates are computed based on Eq. 2. **(d, e, f)** Same as **(a, b, c)** but subtracting the rate of detection by chance. Values that are positive (blue) indicate that XCO_2 anomaly enhancements are better able to detect surface fluxes than by chance.

https://doi.org/10.5194/acp-2022-506
Preprint. Discussion started: 4 August 2022
© Author(s) 2022. CC BY 4.0 License.

Atmospheric Chemistry and Physics Discussions

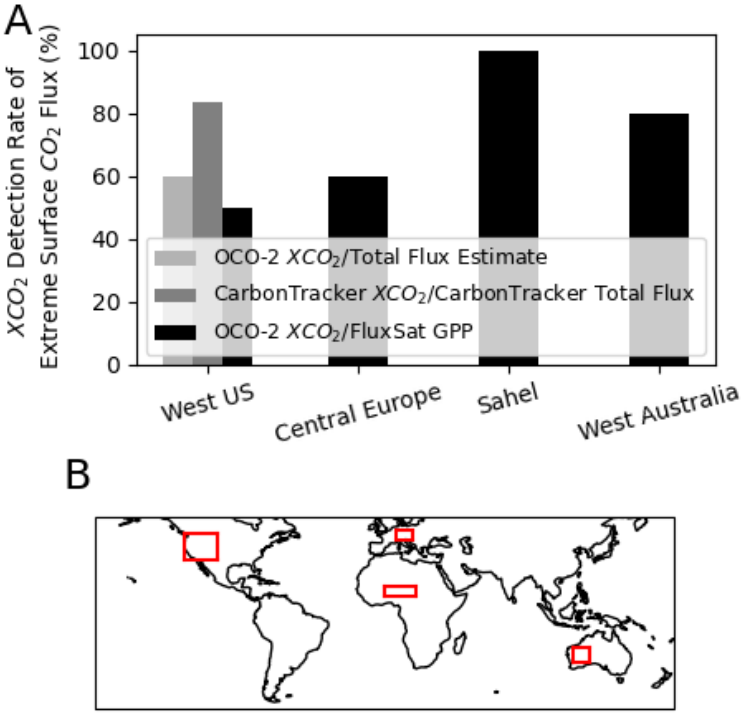

Figure 11. OCO-2 XCO_2 anomalies alone can detect extreme CO_2 fluxes. **(a)** OCO-2 detection rate of extreme surface fluxes (or positive XCO_2 anomalies when surface flux anomalies are the largest). The legend shows the datasets used to estimate the detection rate including pairs of OCO-2 XCO_2 anomalies and total flux estimates from LPJ and QFED, pairs of CarbonTracker XCO_2 anomalies and CarbonTracker total flux estimates, and pairs of OCO-2 XCO_2 anomalies and photosynthesis flux estimates from FluxSat GPP. **(b)** Reference map of regions shown in **(a)**.

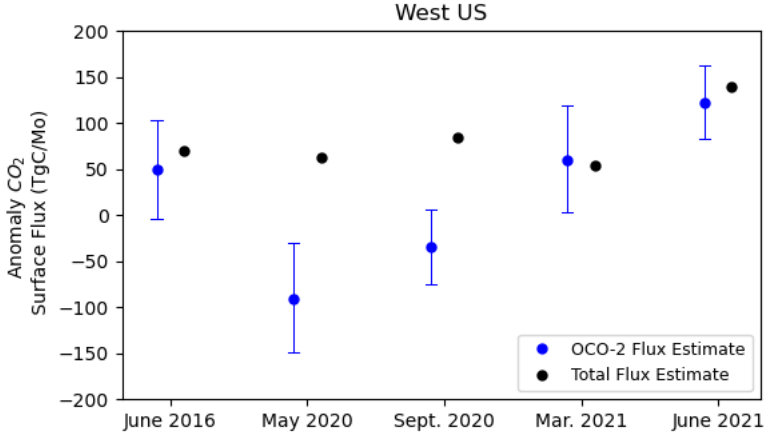

https://doi.org/10.5194/acp-2022-506
Preprint. Discussion started: 4 August 2022
© Author(s) 2022. CC BY 4.0 License.

Atmospheric Chemistry and Physics Discussions

Figure 12. OCO-2 can roughly estimate extreme surface CO_2 fluxes. OCO-2 estimation of extreme surface fluxes in the Western US target domain. Total flux estimates are surface fluxes estimated from a combination of a dynamic global vegetation model (LPJ) and wildfire model reanalysis estimates. Error bars are determined from bootstrapping error estimates determined in Fig. 8c. Fossil fuel anomalies are negligible in magnitude compared to the biosphere and fire sources (see Fig. S1).

595 **4 Conclusions**

We demonstrate that OCO-2 satellite retrieved XCO_2 can be used with mass balance frameworks to detect and estimate biospheric CO_2 flux anomalies at monthly timescales, which exceeds expectations of such greenhouse gas satellites. The application tested here ultimately requires aggregating XCO_2 over regional spatial domains with careful consideration of transport conditions. Namely, the surface flux estimation mass balance method using XCO_2 improves when using larger spatial
600 domains and when wind conditions are on average from the same background location in a given month and flow consistently through the target domain. The larger spatial domain reduces errors due to turbulent atmospheric mixing of surface CO_2 sources that would hinder use of a source pixel mass balance method. Additionally, use of the larger area inherently requires aggregation of several XCO_2 soundings which reduces the magnitude of XCO_2 errors.

605 Satellite XCO_2 anomalies from OCO-2 are particularly useful for evaluating more extreme biosphere fluxes. We show here that the timing and magnitudes of extreme CO_2 fluxes can be monitored where OCO-2 XCO_2 instrument and retrieval error hinder evaluating smaller flux anomalies. In the absence of this error, the performance of these methods greatly improve as suggested by CarbonTracker reanalysis. Therefore, any reduction in XCO_2 measurement and retrieval error in upcoming greenhouse gas missions (i.e., GeoCarb) may extend the ability to globally monitor the timing and magnitude of biosphere
610 anomalies at shorter timescales (beyond that of their design specifications to evaluate aggregated carbon cycle responses at longer than seasonal timescales). Furthermore, even if advection conditions prevent use of the simple pixel source mass balance method, extreme fluxes at least can be detected using only the observed monthly XCO_2 anomaly within the target domain. In addition to the Western US study domain here, this anomaly-only approach is demonstrated in other domains like the Sahel, Europe, and Western Australia that may have more complex advection conditions.

615

The value of such a means to monitor and estimate total surface carbon fluxes is manifold: it is simple in not requiring many assumptions and ancillary datasets; it is rapid and therefore can be used as a first estimate in monitoring extreme events; it uses XCO_2 which integrates all surface CO_2 flux sources, the components of which otherwise need to be estimated separately in bottom-up approaches; since it is based mainly on observations independent of land surface models, it can be used as
620 independent estimate to evaluate global model surface carbon flux outputs.

https://doi.org/10.5194/acp-2022-506
Preprint. Discussion started: 4 August 2022
© Author(s) 2022. CC BY 4.0 License.

Atmospheric Chemistry and Physics Discussions

We recommend that future work determine all global terrestrial ecosystems with favorable wind conditions as defined in the study where the surface carbon flux estimation method can be applied. A particular focus should be placed on tropical locations where measurement networks are sparse with consequently uncertain model outputs as well as where the biosphere takes up the largest proportion of anthropogenic emissions. These methods should also be developed for near real time monitoring in known climate change hotspot regions, as is done here for the Western US hotspot, where more frequent and intense climate anomalies are expected in the future.

5 Code/Data Availability

All datasets used here are freely availability. CarbonTracker reanalysis data (CT2019B) are available at https://gml.noaa.gov/ccgg/carbontracker/. MERRA2 reanalysis wind and pressure fields are available at https://disc.gsfc.nasa.gov/datasets/M2T3NVASM_5.12.4/summary. OCO-2 XCO_2 retrievals and QFED outputs are available at https://disc.gsfc.nasa.gov. The LPJ model code is publicly available at https://github.com/benpoulter/LPJ-wsl_v2.0.

6 Author Contributions

B.P. conceived the study. A.F.F. conducted the analysis and wrote the manuscript. B.P. and A.C. led the study. Z.Z. ran the LPJ model. Y.S. provided GPP remote sensing retrievals and offered guidance on their interpretation. All authors contributed interpretations of figures and textual edits.

7 Acknowledgements

Andrew F. Feldman's research was supported by an appointment to the NASA Postdoctoral Program at the NASA Goddard Space Flight Center, administered by Oak Ridge Associated Universities under contract with NASA.

8 Competing Interests

The authors declare that they have no conflict of interest.

References

Basu, S., Baker, D.F., Chevallier, F., Patra, P.K., Liu, J., Miller, J.B., 2018. The impact of transport model differences on CO2 surface flux estimates from OCO-2 retrievals of column average CO2. Atmos. Chem. Phys. 18, 7189–7215. https://doi.org/10.5194/acp-18-7189-2018

Basu, S., Guerlet, S., Butz, A., Houweling, S., Hasekamp, O., Aben, I., Krummel, P., Steele, P., Langenfelds, R., Torn, M.,

https://doi.org/10.5194/acp-2022-506
Preprint. Discussion started: 4 August 2022
© Author(s) 2022. CC BY 4.0 License.

Atmospheric Chemistry and Physics Discussions

Biraud, S., Stephens, B., Andrews, A., Worthy, D., 2013. Global CO2 fluxes estimated from GOSAT retrievals of total column CO2. Atmos. Chem. Phys. 13, 8695–8717. https://doi.org/10.5194/acp-13-8695-2013

Bovensmann, H., Burrows, J.P., Buchwitz, M., Frerick, J., Noël, S., Rozanov, V. V., Chance, K. V., Goede, A.P.H., 1999. SCIAMACHY: Mission objectives and measurement modes. J. Atmos. Sci. 56, 127–150. https://doi.org/10.1175/1520-0469(1999)056<0127:SMOAMM>2.0.CO;2

Buchwitz, M., Reuter, M., Noël, S., Bramstedt, K., Schneising, O., Hilker, M., Fuentes Andrade, B., Bovensmann, H., Burrows, J.P., Di Noia, A., Boesch, H., Wu, L., Landgraf, J., Aben, I., Retscher, C., O'Dell, C.W., Crisp, D., 2021. Can a regional-scale reduction of atmospheric CO2during the COVID-19 pandemic be detected from space? A case study for East China using satellite XCO2retrievals. Atmos. Meas. Tech. 14, 2141–2166. https://doi.org/10.5194/amt-14-2141-2021

Buchwitz, M., Reuter, M., Schneising, O., Hewson, W., Detmers, R.G., Boesch, H., Hasekamp, O.P., Aben, I., Bovensmann, H., Burrows, J.P., Butz, A., Chevallier, F., Dils, B., Frankenberg, C., Heymann, J., Lichtenberg, G., De Mazière, M., Notholt, J., Parker, R., Warneke, T., Zehner, C., Griffith, D.W.T., Deutscher, N.M., Kuze, A., Suto, H., Wunch, D., 2017a. Global satellite observations of column-averaged carbon dioxide and methane: The GHG-CCI XCO2 and XCH4 CRDP3 data set. Remote Sens. Environ. 203, 276–295. https://doi.org/10.1016/j.rse.2016.12.027

Buchwitz, M., Schneising, O., Reuter, M., Heymann, J., Krautwurst, S., Bovensmann, H., Burrows, J.P., Boesch, H., Parker, R.J., Somkuti, P., Detmers, R.G., Hasekamp, O.P., Aben, I., Butz, A., Frankenberg, C., Turner, A.J., 2017b. Satellite-derived methane hotspot emission estimates using a fast data-driven method. Atmos. Chem. Phys. 17, 5751–5774. https://doi.org/10.5194/acp-17-5751-2017

Butz, A., Guerlet, S., Hasekamp, O., Schepers, D., Galli, A., Aben, I., Frankenberg, C., Hartmann, J. -M., Tran, H., Kuze, A., Keppel-Aleks, G., Toon, G., Wunch, D., Wennberg, P., Deutscher, N., Griffith, D., Macatangay, R., Messe, J., Warneke, T., 2011. Toward accurate CO2 and CH4 observations from GOSAT. Geophys. Res. Lett. 38, L14812.

Byrne, B., Jones, D.B.A., Strong, K., Zeng, Z.C., Deng, F., Liu, J., 2017. Sensitivity of CO2 surface flux constraints to observational coverage. J. Geophys. Res. 122, 6672–6694. https://doi.org/10.1002/2016JD026164

Byrne, B., Liu, J., Lee, M., Yin, Y., Bowman, K.W., Miyazaki, K., Norton, A.J., Joiner, J., Pollard, D.F., Griffith, D.W.T., Velazco, V.A., Deutscher, N.M., Jones, N.B., Paton-Walsh, C., 2021. The carbon cycle of southeast Australia during 2019–2020: Drought, fires, and subsequent recovery. AGU Adv. 2, e2021AV000469.

Chatterjee, A., Gierach, M.M., Sutton, A.J., Feely, R.A., Crisp, D., Eldering, A., Gunson, M.R., O'Dell, C.W., Stephens, B.B., Schimel, D.S., 2017. Influence of El Niño on atmospheric CO2 over the tropical Pacific Ocean: Findings from NASA's OCO-2 mission. Science (80-.). 358. https://doi.org/10.1126/science.aam5776

Chen, Z., Huntzinger, D.N., Liu, J., Piao, S., Wang, X., Sitch, S., Friedlingstein, P., Anthoni, P., Arneth, A., Bastrikov, V., Goll, D.S., Haverd, V., Jain, A.K., Joetzjer, E., Kato, E., Lienert, S., Lombardozzi, D.L., Mcguire, P.C., Melton, J.R., Nabel, J.E.M.S., Pongratz, J., Poulter, B., Tian, H., Wiltshire, A.J., Zaehle, S., Miller, S.M., 2021. Five years of variability in the global carbon cycle: comparing an estimate from the Orbiting Carbon Observatory-2 and process-based

© Author(s) 2022. CC BY 4.0 License.

models. Environ. Res. Lett. 16. https://doi.org/10.1088/1748-9326/abfac1

Chevallier, F., Bréon, F.M., Rayner, P.J., 2007. Contribution of the Orbiting Carbon Observatory to the estimation of CO2 sources and sinks: Theoretical study in a variational data assimilation framework. J. Geophys. Res. Atmos. 112, 1–11. https://doi.org/10.1029/2006JD007375

Chevallier, F., Palmer, P.I., Feng, L., Boesch, H., O'Dell, C.W., Bousquet, P., 2014. Toward robust and consistent regional CO2 flux estimates from in situ and spaceborne measurements of atmospheric CO2. Geophys. Res. Lett. 41, 1065–1070. https://doi.org/10.1002/2013GL058772.Received

Chevallier, F., Zheng, B., Broquet, G., Ciais, P., Liu, Z., Davis, S.J., Deng, Z., Wang, Y., Bréon, F.M., O'Dell, C.W., 2020. Local Anomalies in the Column-Averaged Dry Air Mole Fractions of Carbon Dioxide Across the Globe During the First Months of the Coronavirus Recession. Geophys. Res. Lett. 47. https://doi.org/10.1029/2020GL090244

Ciais, P., Dolman, A.J., Bombelli, A., Duren, R., Peregon, A., Rayner, P.J., Miller, C., Gobron, N., Kinderman, G., Marland, G., Gruber, N., Chevallier, F., Andres, R.J., Balsamo, G., Bopp, L., Bréon, F.M., Broquet, G., Dargaville, R., Battin, T.J., Borges, A., Bovensmann, H., Buchwitz, M., Butler, J., Canadell, J.G., Cook, R.B., Defries, R., Engelen, R., Gurney, K.R., Heinze, C., Heimann, M., Held, A., Henry, M., Law, B., Luyssaert, S., Miller, J., Moriyama, T., Moulin, C., Myneni, R.B., Nussli, C., Obersteiner, M., Ojima, D., Pan, Y., Paris, J.D., Piao, S.L., Poulter, B., Plummer, S., Quegan, S., Raymond, P., Reichstein, M., Rivier, L., Sabine, C., Schimel, D., Tarasova, O., Valentini, R., Wang, R., Van Der Werf, G., Wickland, D., Williams, M., Zehner, C., 2014. Current systematic carbon-cycle observations and the need for implementing a policy-relevant carbon observing system. Biogeosciences 11, 3547–3602. https://doi.org/10.5194/bg-11-3547-2014

Cook, B.I., Ault, T.R., Smerdon, J.E., 2015. Unprecedented 21st century drought risk in the American Southwest and Central Plains. Sci. Adv. 1, 1–7. https://doi.org/10.1126/sciadv.1400082

Crisp, D., Atlas, R.M., Breon, F.M., Brown, L.R., Burrows, J.P., Ciais, P., Connor, B.J., Doney, S.C., Fung, I.Y., Jacob, D.J., Miller, C.E., O'Brien, D., Pawson, S., Randerson, J.T., Rayner, P., Salawitch, R.J., Sander, S.P., Sen, B., Stephens, G.L., Tans, P.P., Toon, G.C., Wennberg, P.O., Wofsy, S.C., Yung, Y.L., Kuang, Z., Chudasama, B., Sprague, G., Weiss, B., Pollock, R., Kenyon, D., Schroll, S., 2004. The Orbiting Carbon Observatory (OCO) mission. Adv. Sp. Res. 34, 700–709. https://doi.org/10.1016/j.asr.2003.08.062

Crisp, D., Pollock, H., Rosenberg, R., Chapsky, L., Lee, R., Oyafuso, F., Frankenberg, C., Dell, C., Bruegge, C., Doran, G., Eldering, A., Fisher, B., Fu, D., Gunson, M., Mandrake, L., Osterman, G., Schwandner, F., Sun, K., Taylor, T., Wennberg, P., Wunch, D., 2017. The on-orbit performance of the Orbiting Carbon Observatory-2 (OCO-2) instrument and its radiometrically calibrated products. Atmos. Meas. Tech. 10, 59–81. https://doi.org/10.5194/amt-10-59-2017

Eldering, A., O'Dell, C.W., Wennberg, P.O., Crisp, D., Gunson, M.R., Viatte, C., Avis, C., Braverman, A., Castano, R., Chang, A., Chapsky, L., Cheng, C., Connor, B., Dang, L., Doran, G., Fisher, B., Frankenberg, C., Fu, D., Granat, R., Hobbs, J., Lee, R.A.M., Mandrake, L., McDuffie, J., Miller, C.E., Myers, V., Natraj, V., O'Brien, D., Osterman, G.B., Oyafuso, F., Payne, V.H., Pollock, H.R., Polonsky, I., Roehl, C.M., Rosenberg, R., Schwandner, F., Smyth, M., Tang, V., Taylor,

© Author(s) 2022. CC BY 4.0 License.

T.E., To, C., Wunch, D., Yoshimizu, J., 2017a. The Orbiting Carbon Observatory-2: First 18 months of science data products. Atmos. Meas. Tech. 10, 549–563. https://doi.org/10.5194/amt-10-549-2017

Eldering, A., Wennberg, P.O., Crisp, D., Schimel, D.S., Gunson, M.R., Chatterjee, A., Liu, J., Schwandner, F.M., Sun, Y., O'Dell, C.W., Frankenberg, C., Taylor, T., Fisher, B., Osterman, G.B., Wunch, D., Hakkarainen, J., Tamminen, J., Weir, B., 2017b. The Orbiting Carbon Observatory-2 early science investigations of regional carbon dioxide fluxes. Science (80-.). 358. https://doi.org/10.1126/science.aam5745

Frank, Dorothea, Reichstein, M., Bahn, M., Thonicke, K., Frank, David, Mahecha, M.D., Smith, P., van der Velde, M., Vicca, S., Babst, F., Beer, C., Buchmann, N., Canadell, J.G., Ciais, P., Cramer, W., Ibrom, A., Miglietta, F., Poulter, B., Rammig, A., Seneviratne, S.I., Walz, A., Wattenbach, M., Zavala, M.A., Zscheischler, J., 2015. Effects of climate extremes on the terrestrial carbon cycle: Concepts, processes and potential future impacts. Glob. Chang. Biol. 21, 2861–2880. https://doi.org/10.1111/gcb.12916

Fraser, A., Palmer, P.I., Feng, L., Bösch, H., Parker, R., Dlugokencky, E.J., Krummel, P.B., Langenfelds, R.L., 2014. Estimating regional fluxes of CO2 and CH4 using space-borne observations of XCH2: XCO2. Atmos. Chem. Phys. 14, 12883–12895. https://doi.org/10.5194/acp-14-12883-2014

Friedlingstein, P., Jones, M.W., Sullivan, M.O., Andrew, R.M., Bakker, D.C.E., Hauck, J., Quéré, C. Le, Peters, G.P., Peters, W., Al, E., 2022. Global Carbon Budget 2021. Earth Syst. Sci. Data 14, 1917–2005.

Gelaro, R., McCarty, W., Suárez, M.J., Todling, R., Molod, A., Takacs, L., Randles, C.A., Darmenov, A., Bosilovich, M.G., Reichle, R., Wargan, K., Coy, L., Cullather, R., Draper, C., Akella, S., Buchard, V., Conaty, A., da Silva, A.M., Gu, W., Kim, G.K., Koster, R., Lucchesi, R., Merkova, D., Nielsen, J.E., Partyka, G., Pawson, S., Putman, W., Rienecker, M., Schubert, S.D., Sienkiewicz, M., Zhao, B., 2017. The modern-era retrospective analysis for research and applications, version 2 (MERRA-2). J. Clim. 30, 5419–5454. https://doi.org/10.1175/JCLI-D-16-0758.1

GMAO, 2015. MERRA-2 inst1_2d_asm_Nx: 2d,1-Hourly,Instantaneous,Single-Level,Assimilation,Single-Level Diagnostics V5.12.4, Greenbelt, MD, USA, Goddard Earth Sciences Data and Information Services Center (GES DISC), Accessed: [01.10.19], 10.5067/3Z173KIE2TPD.

Hakkarainen, J., Ialongo, I., Maksyutov, S., Crisp, D., 2019. Analysis of four years of global XCO2 anomalies as seen by Orbiting Carbon Observatory-2. Remote Sens. 11, 1–20. https://doi.org/10.3390/RS11070850

Hakkarainen, J., Ialongo, I., Tamminen, J., 2016. Direct space-based observations of anthropogenic CO2 emission areas from OCO-2. Geophys. Res. Lett. 43, 11,400-11,406. https://doi.org/10.1002/2016GL070885

Halder, S., Tiwari, Y.K., Valsala, V., Sijikumar, S., Janardanan, R., Maksyutov, S., 2021. Benefits of satellite XCO2 and newly proposed atmospheric CO2 observation network over India in constraining regional CO2 fluxes. Sci. Total Environ. 151508. https://doi.org/10.1016/j.scitotenv.2021.151508

Heymann, J., Reuter, M., Buchwitz, M., Schneising, O., Bovensmann, H., Burrows, J.P., Massart, S., Kaiser, J.W., Crisp, D., 2016. CO2 emission of Indonesian fires in 2015 estimated from satellite-derived atmospheric CO2 concentrations. Geophys. Res. Lett. 44, 1537–1544. https://doi.org/10.1002/2016GL072042.Received

https://doi.org/10.5194/acp-2022-506
Preprint. Discussion started: 4 August 2022
© Author(s) 2022. CC BY 4.0 License.

Atmospheric Chemistry and Physics Discussions

Houweling, S., Baker, D., Basu, S., Boesch, H., Butz, A., Chevallier, F., Deng, F., Dlugokencky, E.J., Feng, L., Ganshin, A., Hasekamp, O., Jones, D., Maksyutov, S., Marshall, J., Oda, T., O'Dell, C.W., Oshchepkov, S., Palmer, P.I., Peylin, P., Poussi, Z., Reum, F., Takagi, H., Yoshida, Y., Zhuravlev, R., 2015. An intercomparison of inversemodels for estimating sources and sinks of CO2 using GOSAT measurements. J. Geophys. Res. 120, 5253–5266. https://doi.org/10.1002/2014JD022962

Irakulis-Loitxate, I., Guanter, L., Maasakkers, J.D., Zavala-Araiza, D., Aben, I., 2021. Satellites unveil easily-fixable super-emissions in one of the world's largest methane hotspot regions [preprint]. Environ. Sci. Technol. 1–32.

Jacob, D.J., Turner, A.J., Maasakkers, J.D., Sheng, J., Sun, K., Liu, X., Chance, K., Aben, I., McKeever, J., Frankenberg, C., 2016. Satellite observations of atmospheric methane and their value for quantifying methane emissions. Atmos. Chem. Phys. 16, 14371–14396. https://doi.org/10.5194/acp-16-14371-2016

Joiner, J., Yoshida, Y., 2021. Global MODIS and FLUXNET-derived Daily Gross Primary Production, V2. ORNL DAAC, Oak Ridge, Tennessee, USA. https://doi.org/10.3334/ORNLDAAC/1835.

Joiner, J., Yoshida, Y., 2020. Satellite-based reflectances capture large fraction of variability in global gross primary production (GPP) at weekly time scales. Agric. For. Meteorol. 291, 108092. https://doi.org/10.1016/j.agrformet.2020.108092

Keppel-Aleks, G., Wennberg, P.O., Washenfelder, R.A., Wunch, D., Schneider, T., Toon, G.C., Andres, R.J., Blavier, J.F., Connor, B., Davis, K.J., Desai, A.R., Messerschmidt, J., Notholt, J., Roehl, C.M., Sherlock, V., Stephens, B.B., Vay, S.A., Wofsy, S.C., 2012. The imprint of surface fluxes and transport on variations in total column carbon dioxide. Biogeosciences 9, 875–891. https://doi.org/10.5194/bg-9-875-2012

Kort, E.A., Frankenberg, C., Costigan, K.R., Lindenmaier, R., Dubey, M.K., Wunch, D., 2014. Four corners: The largest US methane anomaly viewed from space. Geophys. Res. Lett. 41, 6898–6903. https://doi.org/10.1002/2014GL061503.Received

Koster, R.D., Darmenov, A., Silva, A., 2015. The Quick Fire Emissions Dataset (QFED): Documentation of Versions 2.1, 2.2 and 2.4. Volume 38; Technical Report Series on Global Modeling and Data Assimilation.

Kuze, A., Taylor, T.E., Kataoka, F., Bruegge, C.J., Crisp, D., Harada, M., Helmlinger, M., Inoue, M., Kawakami, S., Kikuchi, N., Mitomi, Y., Murooka, J., Naitoh, M., O'Brien, D.M., O'Dell, C.W., Ohyama, H., Pollock, H., Schwandner, F.M., Shiomi, K., Suto, H., Takeda, T., Tanaka, T., Urabe, T., Yokota, T., Yoshida, Y., 2014. Long-term vicarious calibration of GOSAT short-wave sensors: Techniques for error reduction and new estimates of radiometric degradation factors. IEEE Trans. Geosci. Remote Sens. 52, 3991–4004. https://doi.org/10.1109/TGRS.2013.2278696

Lindqvist, H., O'Dell, C.W., Basu, S., Boesch, H., Chevallier, F., Deutscher, N., Feng, L., Fisher, B., Hase, F., Inoue, M., Kivi, R., Morino, I., Palmer, P.I., Parker, R., Schneider, M., Sussmann, R., Yoshida, Y., 2015. Does GOSAT capture the true seasonal cycle of carbon dioxide? Atmos. Chem. Phys. 15, 13023–13040. https://doi.org/10.5194/acp-15-13023-2015

Liu, J., Bowman, K., Parazoo, N.C., Bloom, A.A., Wunch, D., Jiang, Z., Gurney, K.R., Schimel, D., 2018. Detecting drought impact on terrestrial biosphere carbon fluxes over contiguous US with satellite observations. Environ. Res. Lett. 13.

© Author(s) 2022. CC BY 4.0 License.

https://doi.org/10.1088/1748-9326/aad5ef

Liu, J., Bowman, K.W., Schimel, D.S., Parazoo, N.C., Jiang, Z., Lee, M., Bloom, A.A., Wunch, D., Frankenberg, C., Sun, Y., O'Dell, C.W., Gurney, K.R., Menemenlis, D., Gierach, M., Crisp, D., Eldering, A., 2017. Contrasting carbon cycle responses of the tropical continents to the 2015–2016 El Niño. Science (80-.). 358. https://doi.org/10.1126/science.aam5690

Liu, Z., Ciais, P., Deng, Z., Lei, R., Davis, S.J., Feng, S., Zheng, B., 2020. Near-real-time data captured record decline in global CO2 emissions due to COVID-19. arXiv 1–45.

Miller, C.E., Crisp, D., DeCola, P.L., Olsen, S.C., Randerson, J.T., Michalak, A.M., Alkhaled, A., Rayner, P., Jacob, D.J., Suntharalingam, P., Jones, D.B.A., Denning, A.S., Nicholls, M.E., Doney, S.C., Pawson, S., Boesch, H., Connor, B.J., Fung, I.Y., O'Brien, D., Salawitch, R.J., Sander, S.P., Sen, B., Tans, P., Toon, G.C., Wennberg, P.O., Wofsy, S.C., Yung, Y.L., Law, R.M., 2007. Precision requirements for space-based XCO2 data. J. Geophys. Res. Atmos. 112. https://doi.org/10.1029/2006JD007659

Miller, S.M., Michalak, A.M., 2020. The impact of improved satellite retrievals on estimates of biospheric carbon balance. Atmos. Chem. Phys. 20, 323–331. https://doi.org/10.5194/acp-20-323-2020

Nassar, R., Hill, T.G., McLinden, C.A., Wunch, D., Jones, D.B.A., Crisp, D., 2017. Quantifying CO2 Emissions From Individual Power Plants From Space. Geophys. Res. Lett. 44, 10045–10053.

OCO-2-Science-Team, Gunson, M., Eldering, A., 2020. OCO-2 Level 2 bias-corrected XCO2 and other select fields from the full-physics retrieval aggregated as daily files, Retrospective processing V10r, Greenbelt, MD, USA, Goddard Earth Sciences Data and Information Services Center (GES DISC), Accessed: [2021.

Ott, L.E., Pawson, S., Collatz, G.J., Gregg, W.W., Menemenlis, D., Brix, H., Rousseaux, C.S., Bowman, K.W., Liu, J., Eldering, A., Gunson, M.R., Kawa, S.R., 2015. Assessing the magnitude of CO2 flux uncertainty in atmospheric CO2 records using products from NASA's Carbon Monitoring Flux Pilot Project. J. Geophys. Res. Atmos. 120, 734–765. https://doi.org/10.1038/175238c0

Palmer, P.I., Feng, L., Baker, D., Chevallier, F., Bösch, H., Somkuti, P., 2019. Net carbon emissions from African biosphere dominate pan-tropical atmospheric CO2 signal. Nat. Commun. 10, 1–9.

Pandey, S., Houweling, S., Lorente, A., Borsdorff, T., Tsivlidou, M., Anthony Bloom, A., Poulter, B., Zhang, Z., Aben, I., 2021. Using satellite data to identify the methane emission controls of South Sudan's wetlands. Biogeosciences 18, 557–572. https://doi.org/10.5194/bg-18-557-2021

Patra, P.K., Crisp, D., Kaiser, J.W., Wunch, D., Saeki, T., Ichii, K., Sekiya, T., Wennberg, P.O., Feist, D.G., Pollard, D.F., Griffith, D.W.T., Velazco, V.A., De Maziere, M., Sha, M.K., Roehl, C., Chatterjee, A., Ishijima, K., 2017. The Orbiting Carbon Observatory (OCO-2) tracks 2-3 peta-gram increase in carbon release to the atmosphere during the 2014-2016 El Niño. Sci. Rep. 7, 1–12. https://doi.org/10.1038/s41598-017-13459-0

Peters, W., Jacobson, A.R., Sweeney, C., Andrews, A.E., Conway, T.J., Masarie, K., Miller, J.B., Bruhwiler, L.M.P., Pétron, G., Hirsch, A.I., Worthy, D.E.J., Van Der Werf, G.R., Randerson, J.T., Wennberg, P.O., Krol, M.C., Tans, P.P., 2007.

© Author(s) 2022. CC BY 4.0 License.

An atmospheric perspective on North American carbon dioxide exchange: CarbonTracker. Proc. Natl. Acad. Sci. U. S. A. 104, 18925–18930. https://doi.org/10.1073/pnas.0708986104

Philip, S.Y., Kew, S.F., Oldenborgh, G.J. Van, Yang, W., Vecchi, G.A., Anslow, F.S., Li, S., Seneviratne, S.I., Luu, L.N., Arrighi, J., Singh, R., Aalst, V., Hauser, M., Schumacher, D.L., Marghidan, C.P., Ebi, K.L., Vautard, R., Tradowsky, J., Coumou, D., Lehner, F., Rodell, C., Stull, R., Howard, R., Gillett, N., Otto, F.E.L., 2021. Rapid attribution analysis of the extraordinary heatwave on the Pacific Coast of the US and Canada June 2021 . World Weather Attrib. 119–123.

Reichstein, M., Bahn, M., Ciais, P., Frank, D., Mahecha, M.D., Seneviratne, S.I., Zscheischler, J., Beer, C., Buchmann, N., Frank, D.C., Papale, D., Rammig, A., Smith, P., Thonicke, K., Van Der Velde, M., Vicca, S., Walz, A., Wattenbach, M., 2013. Climate extremes and the carbon cycle. Nature 500, 287–295. https://doi.org/10.1038/nature12350

Reuter, M., Bovensmann, H., Buchwitz, M., Burrows, J.P., Connor, B.J., Deutscher, N.M., Griffith, D.W.T., Heymann, J., Keppel-Aleks, G., Messerschmidt, J., Notholt, J., Petri, C., Robinson, J., Schneising, O., Sherlock, V., Velazco, V., Warneke, T., Wennberg, P.O., Wunch, D., 2011. Retrieval of atmospheric CO2 with enhanced accuracy and precision from SCIAMACHY: Validation with FTS measurements and comparison with model results. J. Geophys. Res. Atmos. 116, 1–13. https://doi.org/10.1029/2010JD015047

Reuter, M., Buchwitz, M., Schneising, O., Krautwurst, S., O'Dell, C.W., Richter, A., Bovensmann, H., Burrows, J.P., 2019. Towards monitoring localized CO2 emissions from space: Co-located regional CO2 and NO2 enhancements observed by the OCO-2 and S5P satellites. Atmos. Chem. Phys. 19, 9371–9383. https://doi.org/10.5194/acp-19-9371-2019

Schimel, D., Pavlick, R., Fisher, J.B., Asner, G.P., Saatchi, S., Townsend, P., Miller, C., Frankenberg, C., Hibbard, K., Cox, P., 2015a. Observing terrestrial ecosystems and the carbon cycle from space. Glob. Chang. Biol. 21, 1762–1776. https://doi.org/10.1111/gcb.12822

Schimel, D., Stephens, B.B., Fisher, J.B., 2015b. Effect of increasing CO2 on the terrestrial carbon cycle. Proc. Natl. Acad. Sci. U. S. A. 112, 436–441. https://doi.org/10.1073/pnas.1407302112

Schwalm, C.R., Williams, C.A., Schaefer, K., Baldocchi, D., Black, T.A., Goldstein, A.H., Law, B.E., Oechel, W.C., Paw U, K.T., Scott, R.L., 2012. Reduction in carbon uptake during turn of the century drought in western North America. Nat. Geosci. 5, 551–556. https://doi.org/10.1038/ngeo1529

Schwandner, F.M., Gunson, M.R., Miller, C.E., Carn, S.A., Eldering, A., Krings, T., Verhulst, K.R., Schimel, D.S., Nguyen, H.M., Crisp, D., O'Dell, C.W., Osterman, G.B., Iraci, L.T., Podolske, J.R., 2017. Spaceborne detection of localized carbon dioxide sources. Science (80-.). 358. https://doi.org/10.1126/science.aam5782

Sitch, S., Smith, B., Prentice, I.C., Arneth, A., Bondeau, A., Cramer, W., Kaplan, J.O., Levis, S., Lucht, W., Sykes, M.T., Thonicke, K., Venevsky, S., 2003. Evaluation of ecosystem dynamics, plant geography and terrestrial carbon cycling in the LPJ dynamic global vegetation model. Glob. Chang. Biol. 9, 161–185. https://doi.org/10.1046/j.1365-2486.2003.00569.x

Varon, D.J., Jacob, D.J., McKeever, J., Jervis, D., Durak, B.O.A., Xia, Y., Huang, Y., 2018. Quantifying methane point sources from fine-scale satellite observations of atmospheric methane plumes. Atmos. Meas. Tech. 11, 5673–5686.

© Author(s) 2022. CC BY 4.0 License.

https://doi.org/10.5194/amt-11-5673-2018

Weir, B., Crisp, D., O'Dell, C.W., Basu, S., Chatterjee, A., Kolassa, J., Oda, T., Pawson, S., Poulter, B., Zhang, Z., Ciais, P., Davis, S.J., Liu, Z., Ott, L.E., 2021. Regional impacts of COVID-19 on carbon dioxide detected worldwide from space. Sci. Adv. 7, 1–10. https://doi.org/10.1126/sciadv.abf9415

Williams, A.P., Cook, B.I., Smerdon, J.E., 2022. Rapid intensification of the emerging southwestern North American megadrought in 2021. Nat. Clim. Chang. 2002.

Wunch, D., Wennberg, P.O., Osterman, G., Fisher, B., Naylor, B., Roehl, M.C., O'Dell, C., Mandrake, L., Viatte, C., Kiel, M., Griffith, D.W.T., Deutscher, N.M., Velazco, V.A., Notholt, J., Warneke, T., Petri, C., De Maziere, M., Sha, M.K., Sussmann, R., Rettinger, M., Pollard, D., Robinson, J., Morino, I., Uchino, O., Hase, F., Blumenstock, T., Feist, D.G., Arnold, S.G., Strong, K., Mendonca, J., Kivi, R., Heikkinen, P., Iraci, L., Podolske, J., Hillyard, P., Kawakami, S., Dubey, M.K., Parker, H.A., Sepulveda, E., García, O.E., Te, Y., Jeseck, P., Gunson, M.R., Crisp, D., Eldering, A., 2017. Comparisons of the Orbiting Carbon Observatory-2 (OCO-2) XCO2 measurements with TCCON. Atmos. Meas. Tech. 10, 2209–2238. https://doi.org/10.5194/amt-10-2209-2017

Yin, Y., Byrne, B., Liu, J., Wennberg, P.O., Davis, K.J., Magney, T., Köhler, P., He, L., Jeyaram, R., Humphrey, V., Gerken, T., Feng, S., Digangi, J.P., Frankenberg, C., 2020. Cropland Carbon Uptake Delayed and Reduced by 2019 Midwest Floods. AGU Adv. 1, 1–15. https://doi.org/10.1029/2019av000140

Zabel, F., Putzenlechner, B., Mauser, W., 2014. Global agricultural land resources - A high resolution suitability evaluation and its perspectives until 2100 under climate change conditions. PLoS One 9, 1–12. https://doi.org/10.1371/journal.pone.0107522

Zhang, Z., Zimmermann, N.E., Calle, L., Hurtt, G., Chatterjee, A., Poulter, B., 2018. Enhanced response of global wetland methane emissions to the 2015-2016 El Niño-Southern Oscillation event. Environ. Res. Lett. 13. https://doi.org/10.1088/1748-9326/aac939

Zheng, B., Chevallier, F., Ciais, P., Broquet, G., Wang, Y., Lian, J., Zhao, Y., 2020. Observing carbon dioxide emissions over China's cities and industrial areas with the Orbiting Carbon Observatory-2. Atmos. Chem. Phys. 20, 8501–8510. https://doi.org/10.5194/acp-20-8501-2020